

WICKING IN MULTI-PLY PAPER STRUCTURES WITH DISSIMILAR PLIES

A Thesis
Presented to
The Academic Faculty

By

Patrick McDonald

In Partial Fulfillment
Of the Requirements for the Degree
Master of Science in the
School of Mechanical Engineering

Georgia Institute of Technology
August 2006

WICKING IN MULTI-PLY PAPER STRUCTURES WITH DISSIMILAR PLIES

Approved by:

Dr. Frederick Ahrens, Advisor
Institute of Paper Science and
Technology
Georgia Institute of Technology

Dr. Timothy Patterson, Advisor
Institute of Paper Science and
Technology
Georgia Institute of Technology

Dr. Haskell Beckham
School of Polymer, Textile, and Fiber
Engineering
Georgia Institute of Technology

Dr. Johannes Leisen
School of Polymer, Textile, and Fiber
Engineering
Georgia Institute of Technology

Date Approved: August 23, 2006

Acknowledgements

I would like to thank my advisors, Dr. Fred Ahrens and Dr. Tim Patterson. This investigation was initiated as a result of Fred's observations, and he always had time to answer my questions and point me in the right direction. While Fred was away in France, I relied largely on Tim's help. Tim also taught me in sevewszral courses, teaching me more about the fascinating field of paper science than I ever expected.

Dr. Haskell Beckham and Dr. Johannes Leisen helped greatly with this project, helping me use NMR equipment to study wicking phenomena. Coming from outside the field of paper science, they also brought a fresh perspective to the problem. Both served on my thesis committee, for which I am very grateful.

I must also thank Craig Simile, a former student whose experimental apparatus I inherited, saving me the considerable trouble of constructing one from scratch. Additionally, reading his thesis on wicking experiments in textiles alerted me to experimental pitfalls I may have otherwise stumbled into.

Not all support is technical, and I must thank my parents, Jay and Brigitte, who have always been there when I needed them. Finally, I would like to thank my girlfriend, Sharon Cheong, for supporting me every step of the way.

Table of Contents

Acknowledgements	iii
Table of Contents	iv
List of Tables	v
List of Figures	vi
Symbols and Abbreviations	viii
Summary	x
Chapter 1: Introduction	1
Chapter 2: Background	2
2.1 Wicking Fundamentals	2
2.2 Paper as a Wicking Material	6
2.3 NMR Wicking Tests	11
2.4 Gravimetric Wicking Tests	14
Chapter 3: Experimental Setup	20
Sample Preparation	20
Porometry	23
Gravimetric Experiments	25
Dye Experiments	29
NMR Experiments	30
Chapter 4: Results and Discussion	33
Humidity Testing	33
Gravimetric Wicking Results	35
Porometry Results	44
Results of Dye Experiments	47
NMR Wicking Results	50
Downward Gravimetric Tests	55
Chapter 5: Conclusions	63
Chapter 6: Future Work	64
Appendix A: Modeling	65
Appendix B: MATLAB Code	71
REFERENCES	76

List of Tables

Table 4.3.1 - Average pore size at different pressing levels	46
Table 4.6.1 - Drainage flow rates for varied sample types	56
Table 4.6.2 - Calculated permeability values for varied sample types	59
Table 4.6.3 - Calculated capillary pressure and permeability. The 2-ply capillary...	60

List of Figures

Figure 2.1.1 - Example of vertical wicking race- Smaller pore sample on left	5
Figure 2.2.2 - Micrograph of softwood fibers magnified 100X5	6
Figure 2.2.3 - Micrograph of hardwood fibers magnified 100X5	7
Figure 2.2.4 - Micrograph of paper web structure magnified 250X5	8
Figure 2.2.5 - Structure of fibrils in a paper fiber	9
Figure 2.4.1 - Diagram of downward drainage test with upward and horizontal flow	15
Figure 2.4.2 - Miller's experimental setup.	18
Figure 3.1.1 - Picture of square handsheet mold	20
Figure 3.1.2 - Picture of square press	21
Figure 3.2.1 - Picture of a PMI Porometer ¹⁸	23
Figure 3.2.2 - A constricted pore measured by porometry. D1 will be the measured...	24
Figure 3.3.1 - View of balance, siphon, and reservoir	26
Figure 3.3.2 - Gravimetric wicking setup	28
Figure 3.4.1 - Schematic of the dye experiments to determine direction of fluid transport	29
Figure 3.5.1 - Diagram of NMR experiment	30
Figure 3.5.2 – Close-up of glass tube in NMR experiment	31
Figure 3.5.3 - Orientation of sample for NMR wicking experiments	32
Figure 4.1.1 - Comparison of unconditioned sample and sample conditioned at 90% RH	33
Figure 4.2.1 - %Regain vs. time for varied sample type	35
Figure 4.2.2 - Height vs. time for varied sample type	36
Figure 4.2.3 - Rate of water absorption for varied sample type	37
Figure 4.2.4 - Squared weight vs. time for varied sample type	38
Figure 4.2.5 - % regain vs. height of wicking front	40
Figure 4.2.6 - Variation in weight of inch long segments, vs. height	41
Figure 4.2.7 - Effect of sample thickness on regain	42

Figure 4.2.8 - Result of gravimetric wicking experiment with samples pressed at 45 psi	43
Figure 4.3.1 - Porometry test on softwood sample	44
Figure 4.3.2 - Porometry test on hardwood sample	45
Figure 4.4.1 - Dye experiment result with hardwood ply in dye	47
Figure 4.4.2 - Dye experiment result with softwood ply in dye	49
Figure 4.5.1 - Series of axial NMR images of a two ply sample	50
Figure 4.5.2 - NMR image of two ply sample at $t = 72$ s	51
Figure 4.5.3 - NMR image of two ply sample at $t = 78$ s	52
Figure 4.5.4 - NMR image of two ply sample at $t = 144$ s	52
Figure 4.5.5 - NMR image of two ply sample at $t = 552$ s	53
Figure 4.5.6 - 3-D graph of NMR wicking experiment	54
Figure 4.6.1 - Results of downward wicking tests	55
Figure 4.6.2 - Steady-state downward wicking results	56
Figure 4.6.3 - Results of attempting to use Miller's method to determine permeability and capillary pressure	57
Figure 4.6.4 - Comparison of calculated and actual results for softwood sample	60
Figure 4.6.5 - Comparison of calculated and actual results for hardwood sample	61
Figure 4.6.6 - Comparison of calculated and actual results for 2-ply sample	62

Symbols and Abbreviations

Symbols Used in Gravimetric Wicking Equations

Symbol	Meaning	Units
dL/dt	Flow rate	cm/s
dM/dt	Mass flow rate	mg/s
g	Gravitational constant	cm/s ²
L	Total flow length	cm
L_c	Capillary length	cm
L_D	Downward flow length	cm
L_H	Horizontal flow length	cm
f	Miller's ratio	-
K	Permeability	cm ²
L_O	Initial flow length in Miller's method	cm
L_V	Upward flow length	cm
m_{dry}	Weight of dry sample	g
m_{wet}	Weight of wet sample	g
P_c	Capillary pressure	dyne/cm ²
P_h	Hydrostatic pressure	dyne/cm ²
\bar{p}	Dimensionless pressure parameter	-
Q	Volumetric flow rate	cm ³ /s
\bar{t}	Dimensionless time parameter	-
t	Time	s
u	Superficial velocity	cm/s
w	Width	cm
z	Thickness	mm
β	Angle of sample in Miller's method	-
γ	Surface tension	dyne/cm
ε	Void fraction	-
μ	Viscosity	dyne s/ cm ²
ρ	Density	g/ cm ³

Constants used

Symbol	Meaning	Value
g	Gravitational constant	980 cm/s ²
μ	Viscosity of water	0.01 dyne s/ cm ²
ρ	Density of water	1.0 g/ cm ³
ρ_{cell}	Density of cellulose	1.5 g/ cm ³

Symbols used in NMR equations

Symbol	Meaning
B_0	Magnetic field
$D(r)$	Molecular self diffusion coefficient
G	Magnetic field gradient
I	Signal intensity
r	Spatial coordinate
$T1$	Spin-lattice relaxation time
$T2$	Spin-spin relaxation time
TE	Echo delay time
TR	Relaxation delay time
γ_g	Gyromagnetic ratio
ρ_{spin}	Spin density
ω	Frequency

Summary

The wicking properties of multi-ply paper samples with dissimilar plies were investigated. These materials exhibit wicking performance in excess of either of their individual plies. Samples were produced from a ply of softwood pulp and a ply of hardwood pulp of equal caliper and basis weight. The softwood sample possessed a larger average pore size, a fact verified via porometry. Samples of a single ply were also produced for comparison. The samples were tested using both upward and downward gravimetric wicking tests. There was no saturation gradient observed, however there was a variation in the degree of bulk expansion during wicking. Capillary pressure and permeability for the various sample types were determined from the results of these tests and compared. It is shown that the wicking performance of the two ply sample is comparable to that of a theoretical material with the capillary pressure of the hardwood ply but the permeability of the softwood ply. Wicking in two-ply samples was also observed in an NMR apparatus. This was used to determine that the hardwood ply leads during wicking, and observe the rate of saturation as well as bulk expansion. A third type of experiment tracked the transport of dyed water from one ply to the other, establishing the direction of fluid transport during wicking to be from the softwood ply to the hardwood ply. The theory is proposed, based on these results, that wicking in this type of material consists of a smaller pored leading ply that draws water from a more permeable larger pored material that acts as a moving reservoir.

CHAPTER 1: INTRODUCTION

Wicking performance is an important part of numerous industries, especially the pulp and paper industry. The most obvious example would be paper toweling, where absorption and retention of water is the primary goal. More effective wicking structures could provide either increased performance, or identical performance using less fiber. An understanding of wicking fundamentals could lead to cost-effective means to increase the performance of paper products. On the production side of the pulp and paper industry, better wicking in press felts (assuming as little as a 1% increase in sheet solids) could lead to tens of millions of dollars in energy savings.

Other industries could benefit from improved wicking, such as textiles. The wicking performance of clothing is important to comfort, and high performance sportsgear is specifically designed for better wicking performance. This is both for comfort, and thermal properties of wicking sweat away from the body. Non-wovens may represent an untapped resource of ideas for improved wicking in these applications.

Multi-ply materials for wicking are nothing new. Double or even triple ply toilet paper or paper toweling can be found in any supermarket. What have not been thoroughly investigated, however, are the wicking properties of dissimilar plies. The obvious thing to expect would be performance that was an average of the two plies individually. Instead, however, multi-ply, dissimilar materials can exhibit performance which exceeds that of either individual ply. The purpose of this investigation was to prove, quantify, and explain this behavior.

To this end, a two pronged experimental approach was used. Bulk wicking tests using electronic data collection were used to obtain quantifiable data on the wicking behavior of multi-ply samples, while NMR (nuclear magnetic resonance) equipment was used to see inside of samples during wicking and observe liquid transport. The data from both types of experiments can be combined to assemble a three dimensional picture of how this kind of wicking behavior works.

CHAPTER 2: BACKGROUND

2.1 Wicking Fundamentals

Wicking here will be defined as the capillary flow of liquid in a porous medium. Anyone who has used a paper towel has a certain intuitive understanding of what wicking behavior looks like. Wicking is the transport of liquid through a porous medium in the absence of external pressures. Wicking occurs as a result of capillary forces. These forces have their basis in adhesion, the attraction of molecules in the fluid to those in the solid medium.¹ When adhesion is greater than cohesion (the attraction of liquid molecules to each other) motion will occur as the liquid moves along the wall. This phenomenon is easily seen as the concave meniscus in a glass of water. This is the cause of capillary pressure (P_c), which will cause liquid to penetrate the porous medium.

Opposing this capillary pressure is viscous drag.² Viscous drag will occur based on the viscosity of the fluid, the wettability of the substrate, and the geometry of the pores. These last two factors can be abstracted as the permeability of the material. So, the effect of capillary pressure is to produce a fluid movement proportional to permeability, a property of the substrate, and inversely proportional to viscosity, a property of the fluid. The common unit of permeability is the darcy, equal to 0.987×10^{-12} square meters.³ It is defined as the permeability such that one cubic centimeter of fluid, viscosity of one centipoise, flows one centimeter through one square centimeter of area in one second, when the pressure gradient is 1 atm/cm.

$$\varepsilon \frac{dL}{dt} = \frac{K}{\mu L} P_c \quad (2.1.1)$$

Where K is the permeability, P_c is the capillary pressure, dL/dt is the flow rate, μ is the viscosity

of water, and ε is the void fraction.

L for length (of liquid penetration) appears in the right hand side of the equation because viscous drag increases with length, since the surface area contacting the fluid is increased along with length. In the absence of other phenomena, fluid movement will gradually slow as it penetrates further into the substrate.

For wicking in the vertical direction, a hydrostatic pressure will also act on the fluid, contributing to or detracting from the pressure gradient produced by capillary pressure. The previous equation then becomes:

$$\varepsilon \frac{dL}{dt} = \frac{K}{\mu L} (P_c - P_h) \quad (2.1.2)$$

$$\varepsilon \frac{dL}{dt} = \frac{K}{\mu L} (P_c - L\rho g) \quad (2.1.3)$$

g is the gravitational constant and ρ is the density of water. Once capillary pressure and hydrostatic pressure equalize, wicking will cease.

Comparison of vertical capillary wicking between large and small pored materials is dependent on height, because capillary pressure is acting against gravitational forces. This can be neglected in a case where hydrostatic pressure is much lower than capillary pressure, as is the case shortly after the beginning of wicking. The easiest way to compare the behavior of fluid in different size pores is to examine circular channels of radius R and length L .^{1,4} Starting with Poiseuille's Law for volume flow rate of a viscous fluid through a circular tube

$$\frac{dV}{dt} = \frac{\pi R^4}{8\mu L} P \quad (2.1.4)$$

and assuming only capillary pressure, we divide by the area πR^2 to get a linear flow rate

$$\frac{dL}{dt} = \frac{R^2}{8\mu L} P_c \quad (2.1.5)$$

The capillary pressure is equivalent to

$$P_c = \frac{2\gamma}{R} \quad (2.1.6)$$

Where γ is the surface tension.

Substituting 2.1.5 into 2.1.4 and integrating yields the Washburn equation³

$$L^2 = \frac{\gamma R}{2\mu} t \quad (2.1.7)$$

In the absence of hydrostatic pressure, a larger pore will wick more quickly early in wicking.

In the general case of vertical wicking, the hydrostatic pressure must be accounted for, giving

$$\frac{dL}{dt} = \frac{R^2}{8\mu L} \left(\frac{2\gamma}{R} - P_H \right) \quad (2.1.8)$$

substituting $P_H = L\rho g$,

$$\frac{dL}{dt} = \frac{1}{\mu} \left(\frac{2\gamma R - L\rho g R^2}{8L} \right) \quad (2.1.9)$$

rearranging, and integrating,

$$\frac{16\gamma R}{(\rho g R^2)^2} \ln \left[\frac{2\gamma}{2\gamma - \rho g R L} \right] - \frac{8L}{\rho g R^2} = \frac{1}{\mu} t \quad (2.1.10)$$

For a known liquid (water) this gives a relationship between R , L , and t . The end result is faster wicking initially for the large pore, but higher capillary pressure in the small pore will allow it to overtake the large pore after a certain period of time. If the large and small pored structures are connected, the difference in capillary pressure will tend to cause liquid transfer from the large to the small pored structure. Additionally any difference in hydrostatic pressure (caused by a

difference in height) will affect the exchange of liquid. Initially, this will act to transfer liquid from the large pored structure to the small (adding to the pressure gradient). After the smaller pored structure has overtaken the large, the pressure difference will act in the opposite direction, against transfer. Theoretically, the height difference after a long time will be sufficient to produce a difference in hydrostatic pressure equal to the difference in capillary pressure. The small pored structure's lead would then remain constant. Figure 2.1.1 shows an example of the changing lead between a large and small pored sample.

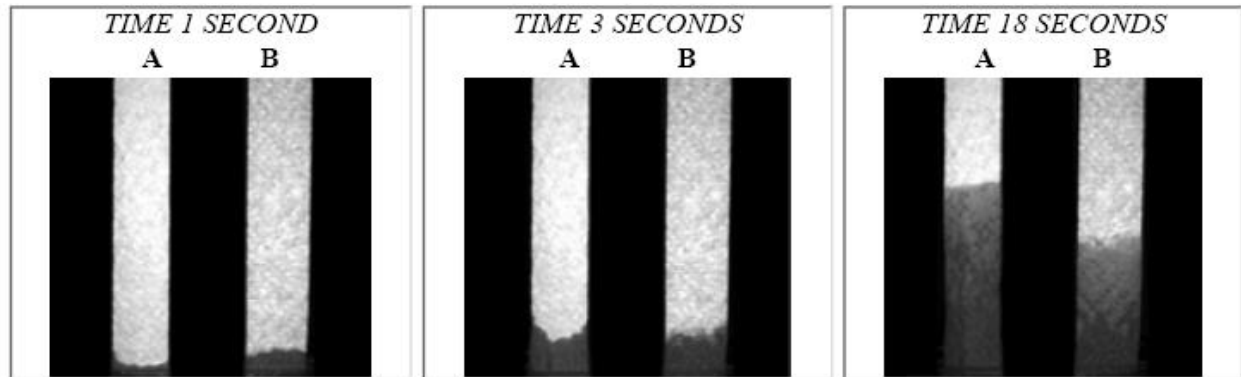


Figure 2.1.1 – Example of vertical wicking race. Smaller pore sample on left.⁴

2.2 Paper as a Wicking Material

Paper as a material comes in a wide variety of types, but some common features are universal. Paper is composed of layered cellulose fibers obtained from wood or other plant materials. The length, stiffness, and diameter of the fiber will affect the properties of the finished product.⁵



Figure 2.2.2 –Micrograph of softwood fibers magnified 200X⁵

Paper fibers can be divided into two primary categories, softwood and hardwood. Softwood fibers are generally longer, between 2-5 mm in length, and coarser (see Figure 2.2.2). The shorter hardwood fibers are usually 1-2 mm in length⁵ (see Figure 2.2.3). This difference in length will affect the structure of a paper sheet. The longer softwood fiber will, as it settles, lie across a larger number of fibers, and generally create a “fluffier” matrix. The shorter hardwood fibers will be more densely packed. Compared to hardwood, softwood paper will have a larger average pore size.

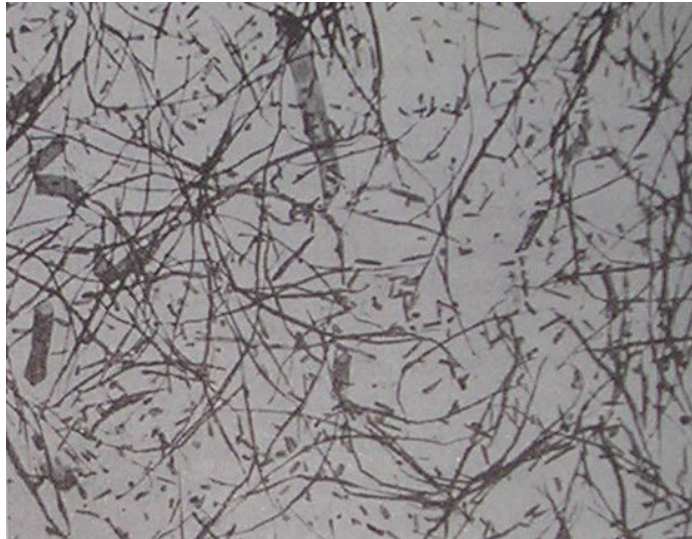


Figure 2.2.3 – Micrograph of hardwood fibers magnified 200X⁵

Far more goes into determining the structure of paper than just fiber choice, of course. The way in which fibers are laid, pressed, and dried will have a major effect on pore structure. Paper made via a handsheet process will have isotropic in-plane properties, while that made on a Fourdrinier machine will have fibers disproportionately oriented in the machine direction.⁵ Increased pressing will reduce the caliper (thickness) of paper, both by flattening fibers and pressing them closely together. Finally, drying processes can result in shrinkage if the paper is not restrained.⁶ An example of a paper structure is given in Figure 2.2.4.

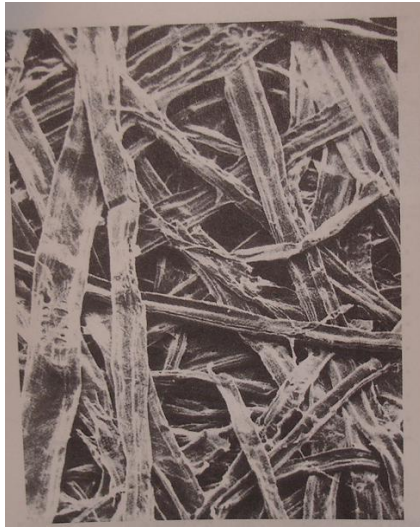


Figure 2.2.4 – Micrograph of paper web structure magnified 250X⁵

Paper, as a wicking material, is significantly more complex than circular tubes. Paper does not have a uniform pore size, but rather a pore size distribution.⁷ Nor are these pores oriented in a single direction. Use of the word “pore” suggests a channel in an otherwise solid object, but the structure of paper is of a densely layered network of fibers, with the gaps between them forming an extremely irregular network of voids. Within a small area of a paper sheet, varied pore size will produce an uneven wicking front.^{1,8} When dealing with paper, it is possible to determine an average equivalent pore size, but as with any statistical average, a sufficiently large number of pores must be measured to do so.

On a small scale, the paper fibers themselves are capable of holding water, as it is absorbed between fibrils⁹ (see Figure 2.2.5). The fiber is like a collection of very small capillaries, in contrast to the larger pores that exist between fibers.¹⁰ Further complicating matters is the hydrogen bonds that hold the fiber network together, and which can be broken apart by water. As the paper is wetted, plasticization will occur. Fiber swelling and bulk

expansion will occur as a result of wetting.^{7,9} So the size and shape of the pore network will change in the region behind the wicking front. This behavior is not accounted for in the traditional models of porous media.¹⁰

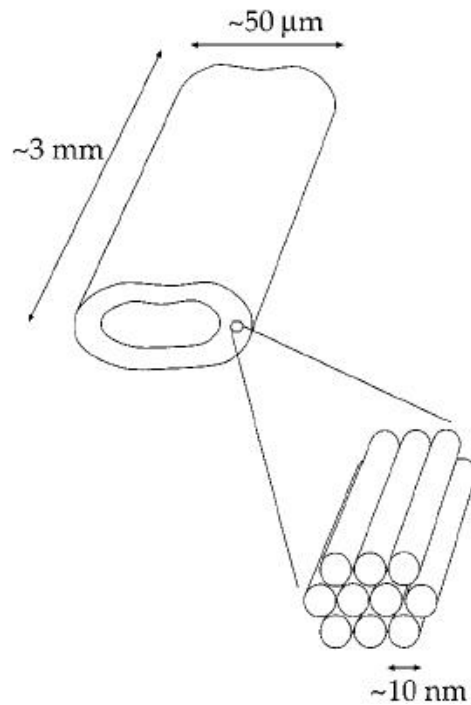


Figure 2.2.5 – Structure of fibrils in a paper fiber⁸

In some porous material with a pore size distribution, such as fabric yarns, a decrease in filling fraction (the fraction of void space that is filled with water) is seen at higher heights during vertical wicking. This occurs as larger pores become unable to wick moisture, due to hydrostatic pressure, leaving only the small pores to make up the wicking front.¹² So the rate of height increase accelerates relative to the rate of weight increase. This behavior should not be expected in paper. Paper is not composed of channels of varied pore sizes that remain constant for each pore. Rather, it presents a rough network of pores; with the size of each individual pore constantly changing.¹³ While complex equations exist for dealing with variable size channels, their utility is limited; it is easier if an equivalent capillary radius can be deduced from other parameters.^{2,11} A closer determination can be done if the characteristic diameter is separated

into a viscous drag diameter and a capillary suction diameter.¹³

Additionally, paper is isotropic (in plane), with as many horizontal channels as vertical. Communication between pores will serve to equalize the wicking front. Considering the wide variation in pore sizes and the frequent changes in pore size, it is unlikely that a wicking path could be easily found that passed solely through narrow pores.¹³ So an analogy to varied sizes of capillary tubes will break down quickly when dealing with complex paper structure.

A theory explaining the enhanced wicking of dissimilar plies can be constructed. The larger capillary pressure of the smaller pored material draws on the reservoir formed by the larger pored material. The reduced viscous drag in the larger pored material provides an easier path for the liquid than would be possible using only the smaller pored material. The increased wicking speed of the large pored structure early on is combined with the increased speed of the small pored structure over a longer period.

2.3 NMR Wicking Tests

Nuclear magnetic resonance (NMR) is a phenomenon that occurs when atomic nuclei in a static magnetic field are exposed to an oscillating magnetic field. This phenomenon is dependent on the spin of the nucleus. A nucleus with a spin of zero will not be detectable via NMR. Most elements have isotopes with non-zero spin, but unless the concentration of these isotopes is sufficiently high, the material will not be detected. Different materials will resonate with varied intensity, allowing them to be differentiated.¹³

Some nuclei, such as those of hydrogen, will separate into two discrete states based on the strength of the magnetic field. The energy difference between these states is constant. The signal from nuclear magnetic resonance occurs as these states transition when exposed to radiation in the RF range. Because the population of the two states is not equal, a net magnetization vector is produced. The frequency ω is given by^{14,15}

$$\omega = -\gamma_g B_0 \quad (2.3.1)$$

Where γ_g is the gyromagnetic ratio and B_0 is the magnetic field.

Using multiple coils, a magnetic field gradient can be created. This creates a linear variation in the magnetic field. Because the resonance frequency is proportional to the strength of the magnetic field, a spatial dependence is introduced.

$$\omega(r) = \left[-\gamma_g (B_0 + rG_r) \right] \quad (2.3.2)$$

Where G_r is the magnetic field gradient.

By varying the orientation of this gradient, a set of data is produced that can be assembled into a magnetic resonance image (MRI). One technique for assembling such an image is the spin-echo technique. Two parameters that are varied in the application of this technique are echo time (TE) and recovery time (TR). The intensity (I) of each pixel in the

resonance image is dependent on these parameters, and the contrast between pixels is given by the following relationship¹⁵

$$I(r) \propto \rho_{spin}(r) F_1[TR, T_1(r)] F_2[TE, T_2(r)] F_3[TE, G, D(r)] \quad (2.3.3)$$

Where $\rho_{spin}(r)$ is the spin density, which is proportional to the number of active nuclei, i.e., the amount of water. It is therefore the quantity which will be needed to characterize the distribution of moisture in the sample being considered. There are, however, several attenuation factors that will affect the contrast and need to be either reduced or accounted for, the F terms in the equation above.

The F_1 contrast function is a result of T_1 relaxation. This is the time taken for the Z magnetization component to return to equilibrium, and is caused by interactions between the nuclei and the rest of the sample.^{14,15}

$$F_1[TR, T_1(r)] = 1 - \exp[-TR/T_1(r)] \quad (2.3.4)$$

As you can see, this attenuation can be eliminated if TR , the repetition time, is much greater than T_1 . So in many cases this attenuation can be ignored completely. However, if the phenomenon under study occurs quickly, it may be necessary to sacrifice contrast in order to increase temporal resolution.

Also present is attenuation from T_2 relaxation. This is the time taken for a return to equilibrium of the transverse magnetization components, and is caused by internuclear interactions.^{15,16}

$$F_2[TE, T_2(r)] = 1 - \exp[-TE/T_2(r)] \quad (2.3.5)$$

This can be reduced by setting TE as short as possible. It cannot be totally eliminated during the standard spin echo sequence, due to limitations of the hardware.

The final type of attenuation (F_3) is caused by molecular diffusion, and like the F_2

attenuation, cannot be eliminated.

NMR has been applied to paper in various contexts, including the examination of drying or moisture adsorption. Topgaard and Sodermann used NMR in order to examine water diffusion into cellulose walls.⁹ They used NMR to see how water is absorbed into the capillaries between the fibrils of a cellulose fiber. This phenomenon occurs on a smaller scale than bulk wicking, but can affect wicking behavior. Harding et al. used NMR to look at water transport during drying in liquid packaging board.¹⁶ They used NMR to view the moisture distribution inside of the drying sheet, and compared results to those of bulk drying tests. The NMR results were found to correlate well with the results of traditional drying tests, while providing insight into the kinetics by showing how moisture distribution varied with time. While applied to a different problem, the motivation mirrors that for applying NMR to wicking experiments.

Work has been done recently applying NMR to the study of wicking in materials other than paper. Leisen and Beckham have used NMR to look at wicking kinetics in nonwoven felts which are used in incontinence products. They found a highly irregular wicking front as a result of the irregular pore structure and the deformability of pores. Paper presents similar irregularities, however the structure of paper is denser and stiffer, so the irregularities will be on a smaller scale.

2.4 Gravimetric Wicking Tests

Vertical, upward wicking tests are commonly used in industry to evaluate wicking performance. In such a test, one end of a sample is dipped in a fluid, usually water, and the time required for the water to reach a certain height is recorded. While useful for rough comparisons, as well as easy to perform, this kind of test nevertheless presents problems. The basic assumption contained in such a test is that the effect of gravity on wicking can be ignored. While in some materials gravitational effects will be similar, the relation between capillary diameter, capillary pressure, and viscosity mean that wicking performance will generally vary with height. So a vertical wicking test designed to compare materials will produce different results based on the target height chosen.⁴

Use of a downward drainage test (see Figure 2.4.1) can determine permeability where it cannot be determined analytically. This test involves letting a sample wick vertically, horizontally, and then downward until it is fully saturated. The sample then becomes essentially a siphon, transporting water at a constant rate. This is especially useful for a material such as paper where sample geometry is both irregular and difficult to precisely determine. Even more useful is that this information can be combined with that obtained from vertical wicking to determine capillary pressure. All unknown properties can be determined experimentally from these techniques. Provided the height of vertical rise (and length of horizontal flow) prior to downward drainage is very small, the downward flow rate will soon reach a steady state limited solely by viscous drag. It does not vary with height or the length of the downward leg.

Downward drainage is used to determine the volume flow rate of water, given by the equation.

$$Q = (zw)u \quad (2.4.1)$$

Where z is thickness, w is width, and the superficial velocity u is based on permeability,

viscosity, fluid density, and the gravitational constant.

$$u = \frac{K}{\mu} \rho g \quad (2.4.2)$$

Permeability is the only unknown quantity, assuming water as the fluid and standard temperature and pressure. However, it is very difficult to design an experimental setup such that downward drainage follows this equation, and there will usually be some length of upward and horizontal flow involved.

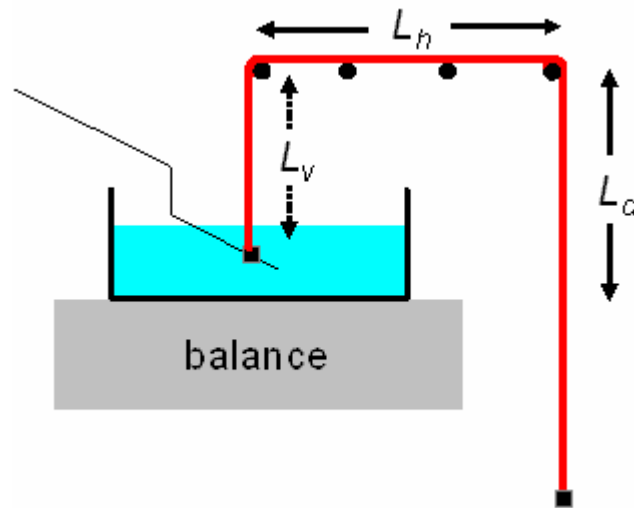


Figure 2.4.1 – Diagram of downward drainage test with upward and horizontal flow.

$$u = \frac{K}{\mu L} P \quad (2.4.3)$$

L is the total length of the sample

$$L = L_v + L_h + L_d \quad (2.4.4)$$

And the pressure is simply the hydrostatic pressure (assuming the full length has been wetted)

$$P = \rho g L_d \quad (2.4.5)$$

So the equation for flow is

$$u = \frac{K \rho g L_d}{\mu L} \quad (2.4.6)$$

If there is no vertical or horizontal leg, the equation reduces to 2.4.2

Two more parameters are needed to calculate capillary pressure; the void fraction and the height of vertical rise early during vertical wicking. Void fraction is easily determined based on sample dimensions and weight, and the density of cellulose. Once all these parameters are known, a relation between height squared and time is used to find capillary pressure. This relation is derived from two dimensionless parameters.

$$\bar{p} = \frac{\rho g L}{p_c} \quad (2.4.7)$$

The dimensionless pressure \bar{p} is the ratio of hydrostatic and capillary pressure. It is zero at time zero as height is zero. The second dimensionless parameter is the dimensionless time parameter \bar{t}

$$\bar{t} = \frac{K p_c^2 g^2}{\varepsilon p_c \mu} t \quad (2.4.8)$$

The utility of these parameters comes from the relation

$$\frac{d\bar{p}^2}{d\bar{t}} = 2(1 - \bar{p}) \quad (2.4.9)$$

as mentioned above,

$$\bar{p}(0) = 0 \quad (2.4.10)$$

so at time zero

$$\frac{d\bar{p}^2}{d\bar{t}} = 2 \quad (2.4.11)$$

So when pressure head is negligible,

$$\bar{p}^2 = 2\bar{t} \quad (2.4.12)$$

or

$$\frac{\rho g^2 L^2}{p_c^2} = 2 \frac{K \rho^2 g^2 t}{\varepsilon p_c \mu} \quad (2.4.13)$$

$$L^2 = \frac{2K p_c}{\varepsilon \mu} t \quad (2.4.14)$$

giving the equation for capillary pressure,

$$p_c = \frac{L^2}{t} \frac{\varepsilon \mu}{2K} \quad (2.4.15)$$

Because the characteristic length (length at which head equals capillary pressure) is relatively high for paper, this relation can be used to determine capillary pressure via a combination of downward drainage and vertical wicking tests.

Miller has provided a series of equations for determining permeability and capillary pressure using solely downward wicking tests.⁴ He used a setup with slanted vertical wicking followed by downward wicking, depicted in Figure 2.4.2.

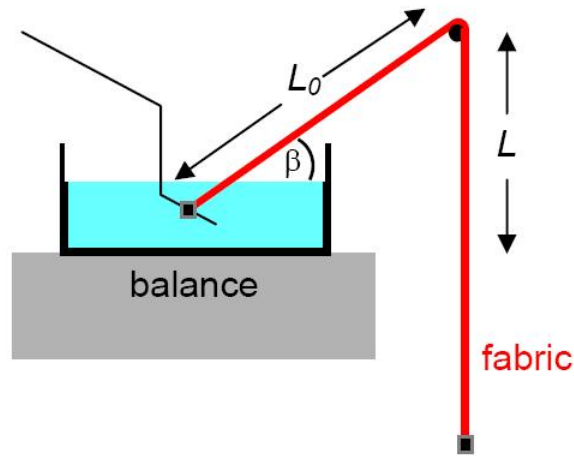


Figure 2.4.2- Miller's experimental setup.

He starts with Darcy's law, and uses the concept of capillary length (L_c) to combine capillary and hydrostatic pressures. Capillary length is the height at which capillary pressure equals hydrostatic pressure, and is proportional to capillary pressure.

$$\frac{dL}{dt} = \frac{\rho g K}{\mu} \left(\frac{L_c - L_0 \cos \beta + L}{L_0 + L} \right) \quad (2.4.16)$$

When the upward and downward lengths are equal,

$$\frac{dL}{dt} = \frac{\rho g K}{\mu} \left[\frac{L_c + 1 - \cos \beta}{L_0} \right] \quad (2.4.17)$$

Changing only the upward length will yield a different constant flow rate. The ratio of these flow rates can be used to determine capillary length, and thenceforth, permeability.

$$f = \left[\frac{dL}{dt} \right]_1 / \left[\frac{dL}{dt} \right]_2 = \left(\frac{L_c + 1 - \cos \beta}{L_{01}} \right) / \left(\frac{L_c + 1 - \cos \beta}{L_{02}} \right) \quad (2.4.18)$$

$$f \left(\frac{L_c}{L_{02}} \right) - \frac{L_c}{L_{01}} = (f - 1)(\cos\beta - 1) \quad (2.4.19)$$

$$L_c = \frac{(f - 1)(\cos\beta - 1)}{fL_{01} - L_{02}} (L_{02}L_{01}) \quad (2.4.20)$$

With capillary length, permeability can be found using either flow rate.

$$K = \frac{2\mu L_0}{\rho g} \left(\frac{1}{L_c - L_0 \cos\beta + L_0} \right) \frac{dL}{dt} \quad (2.4.21)$$

The same basic principle can be modified to include numerous experiments by plotting the flow rates versus $1/L_0$. Performing a linear regression on these data points gives a graph whose slope should be equal to

$$\frac{\rho g K L_c}{2\mu} \quad (2.4.22)$$

and y-intercept equal to

$$\frac{\rho g K}{2\mu} (1 - \sin\beta) \quad (2.4.23)$$

The y-intercept found by linear regression is plugged into equation 2.4.19, and permeability solved for. The slope found by linear regression is plugged into equation 2.4.18 along with this permeability. Capillary length is solved for and converted to capillary pressure.

CHAPTER 3: EXPERIMENTAL SETUP

3.1 Sample Preparation



Figure 3.1.1 – Picture of square handsheet mold

Samples were prepared following a modified TAPPI procedure 295 in an 8 x 8 inch handsheet mold (see Figure 3.1.1). Fifty grams each of softwood and hardwood drylap pulp (bleached and chemically refined) were disintegrated and diluted in 10 liters of water. For a normal sample, 2 liters of the disintegrated pulp were used. After being couched, samples were stacked between sheets of blotter and pressed in a manually operated hydraulic press (see Figure 3.1.2). Most samples were pressed 20 seconds at 20 psi. Some additional samples were prepared at 45 and 80 psi, pressed for about 2 minutes. After pressing, samples were dried under constraint on a heated cylinder.

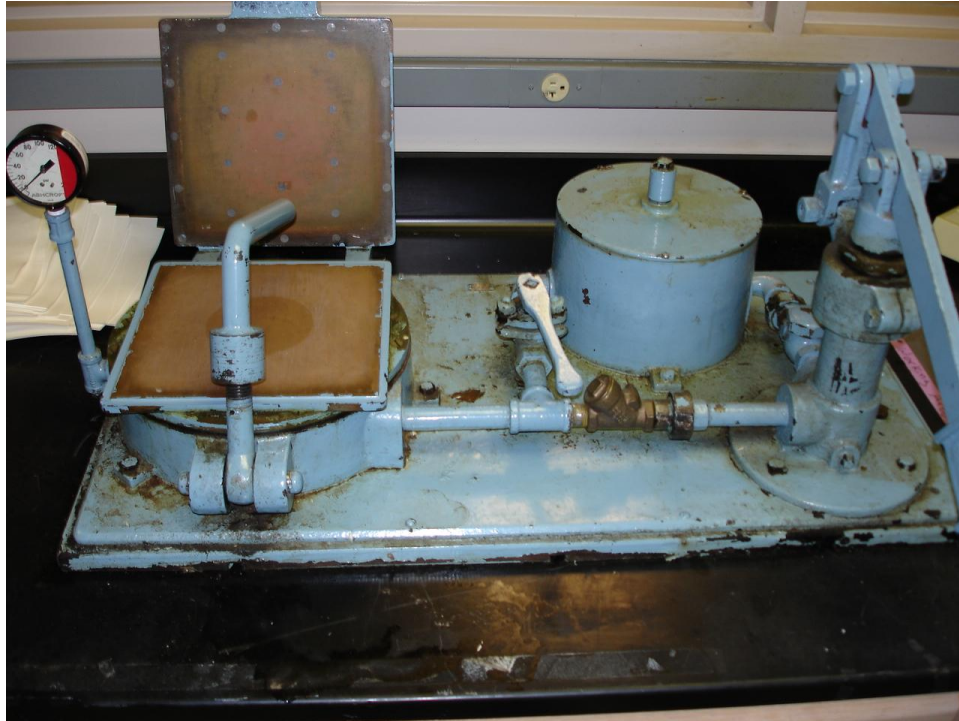


Figure 3.1.2 - Picture of square press.

For two ply samples, one liter of disintegrated pulp was used in the mold to produce a sample at half regular basis weight. One ply of each material was made. The wet samples were then pressed together and dried as described above, producing a layered material with two distinct plies.

Thickness of each sample handsheet was measured using a soft platen caliper test. Air permeability was measured via a standard Gurley test (TAPPI procedure 460). The Gurley test consists of measuring the time required to force a known quantity of air through a paper sample with a known pressure. While not directly applicable to permeability of a wet sample, differences between samples could be compared qualitatively and consistency checked.

Dry weight of the standard handsheet was about 9 grams, for a basis weight of 225 g/m². For bulk wicking tests, these handsheets would normally be cut into either 10 or 20 cm strips.

Width was uniformly about 2.5 cm. Some small variations in dimension existed, but were compensated for during analysis by analyzing regain instead of weight. Regain is defined as the weight of water absorbed divided by the initial dry weight of the sample.

3.2 Porometry



Figure 3.2.1 – Picture of Porous Materials Inc. Porometer¹⁷

An additional piece of equipment used to test these handsheets was a Porous Materials Inc. 1100-AEX capillary flow porometer, an example of which is shown in Figure 3.2.1. This device attempts to determine the pore size distribution of a sample. A sample is placed in the device, and air is blown through it at increasing pressures. The machine records the pressure and the volume of air used. The sample is then treated with a non evaporative liquid such as PoreWick, which has a surface tension of 16 dyne/cm. The pressure is again gradually raised. The largest pores will be the first to be emptied as a result of this pressure. As pressure increases, smaller pores will empty. Comparison with the pressure/ air volume curve of the dry sample allows for a determination of approximate pore sizes.¹⁷

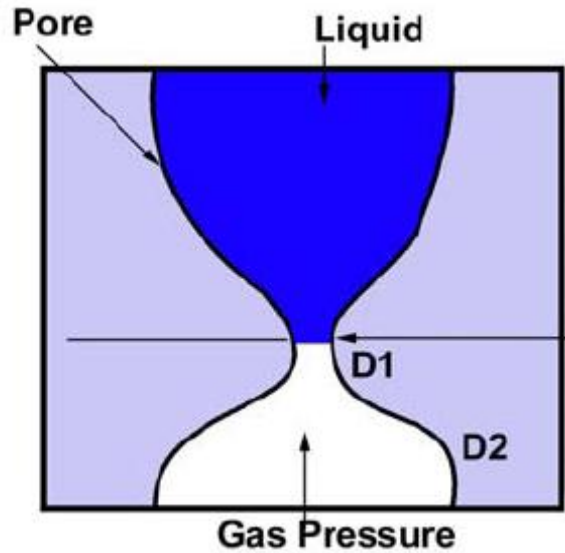


Figure 3.2.2 - A constricted pore measured by porometry. D1 will be the measured diameter. ¹⁷

There are several problems with this device, however. For one, it makes assumptions of constant pore size and circular pores, neither of which is true for paper. The problem with the constant pore size assumption can be seen in Figure 3.2.2. The PoreWick liquid does not interact chemically with paper the way water does, so the plasticization and expansion integral to the wicking properties of paper are not accounted for. The use of water as a wicking fluid is problematic because of the effect of evaporation. A better method for simulating a wet web is to freeze dry the sample and then use the PoreWick fluid. Even with this technique, reproducibility remained a problem. The device is not completely useless, however. It can be used to compare samples and get a very rough estimate for pore size differences. Attempting to use it to establish accurate, quantitative results for pore size distributions would not be particularly wise, unfortunately.

3.3 Gravimetric Wicking Setup

Exploratory experiments into 2-ply wicking were basic, and conducted by visually inspecting wicking in pieces of drylap pulp. To roughly simulate a multi-ply situation, dissimilar samples were clamped together between two pieces of plexiglas. Height versus time measurements were made by visual inspection. The advantage of the two ply material was visible, but the setup had too many flaws for an in depth analysis. This was not a good simulation of paper wicking, as the plexiglas clamp prevented bulk expansion of the paper samples. Removing the plexiglas, however, introduced evaporative effects. The interface between samples was also less than optimal, which eventually led to the creation of custom made multi-ply samples as described above. A better setup was needed, which included humidity control and a more precise measurement system. Fortunately, such a setup already existed from previous experiments in fabrics¹² and was easily modified.

The experimental setup used for vertical wicking tests was contained in a cubic plexiglas environmentally controlled chamber. The container was raised and lowered via a winch. A household humidifier and an aquarium pump were used for humidity control. An RH probe was used to monitor changes in relative humidity. During experiments, relative humidity was raised to about 90% through the use of the humidifier. Once elevated, the humidity was maintained at this level with the use of the small aquarium pump. The larger humidifier was turned off during experiments to prevent the airflow from its fan from affecting the scale. Temperature is maintained constant at 72°F.

This elevated humidity was necessary to prevent evaporative effects from affecting wicking behavior. Evaporation from the sample would exaggerate the weight of water absorbed by the sample. Elevated humidity solves the problem of evaporation, but can add the problem of absorption. Rather than allowing the sample to absorb moisture during the experiment, handsheets to be tested were left in the chamber at 90% humidity for one hour prior to the

beginning of experiments. This allowed for the fibril voids to become fully saturated, but not the spaces between fibers.⁹ This ensures that the sample will not absorb any moisture from the air during the run itself, and that the initial moisture content of the samples is the same for all experiments. Otherwise, initially dry samples would absorb more total water than samples with the same pore structure but greater initial water weight.



Figure 3.3.1 - View of balance, siphon, and reservoir

A water reservoir, initially empty, was supported by an electronic scale (a Sartorius BP 310 S), as seen in Figure 3.3.1. A paper sample was suspended vertically above this reservoir with the bottom close to but not touching the bottom of the reservoir. The purpose of the scale is to allow electronic data collection. There are two advantages to this method. For one, the scale

is more sensitive to minute changes than the human eye, allowing for more accurate measurement. Additionally, height and weight may not necessarily correlate in linear fashion. The weight based measurement may be combined with visual measurement to determine this relationship. Note that it is critical that the sample not touch the bottom of the reservoir. If it does, both the sample and the water within will be detected by the scale, reducing the apparent weight of water wicked.

Prior to each run, the length, width, and weight of the paper sample used were recorded. Most samples were about 10 cm long and 2.5 cm wide. During an experimental run, the reservoir was filled with water through a rubber tube passing through the plexiglas enclosure from an external container equipped with a stopcock. An external container is necessary to prevent humidity loss from occurring when the chamber is opened. Once the water level rose to the bottom of the paper, the flow of water to the reservoir was stopped. The scale was then zeroed and the data collection begun. Recording usually began about 3 seconds after the start of wicking.

Weight and time data were automatically collected using a laptop computer and BalanceTalk XL software, produced by Labtronics. This software allows a computer to communicate with a balance via an RS-232 cable. The balance can be remotely zeroed, and the command to begin transmitting data can be given by computer. This is necessary, as the balance is inaccessible during experimentation, as seen in Figure 3.3.2. The BalanceTalk software relays time and weight data directly to a Microsoft Excel spreadsheet.

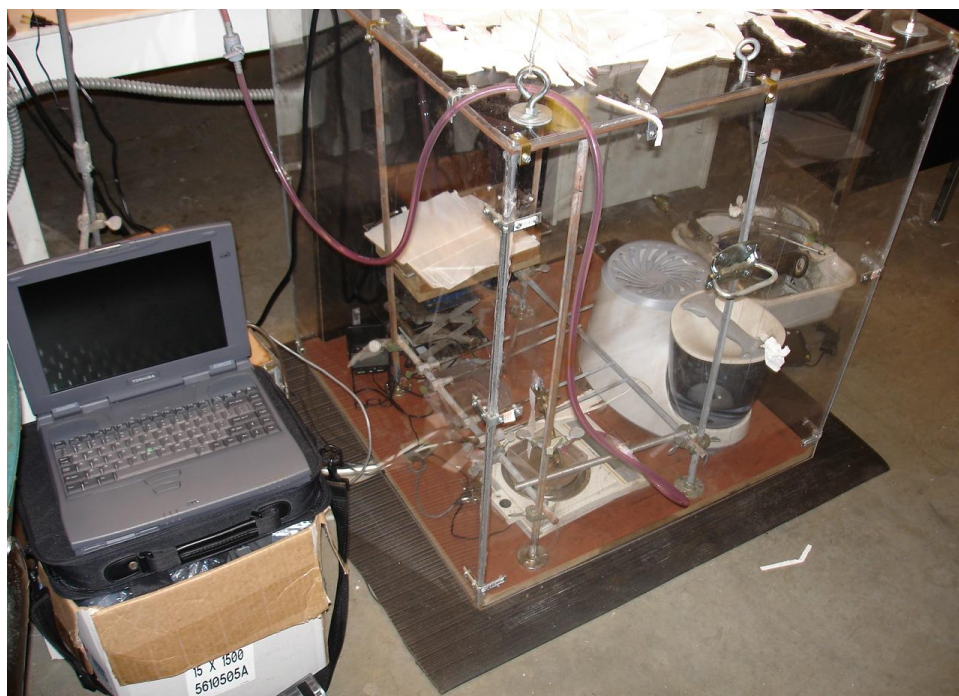


Figure 3.3.2 - Gravimetric wicking setup

When the experiment was stopped, the wet weight and, if applicable, height of water absorption, were measured. In most cases, the experiment was not stopped until the sample had wicked completely.

Experiments were also conducted in which the height of the wicking front was measured vs time. This was done simply by marking the sample at various heights and recording the time taken to reach these heights. This was done simultaneously with weight measurements, to allow for comparison. Sample length did not change significantly as a result of wetting.

Downward drainage tests were conducted in a similar manner to the upward tests. The sample was bent in two places and held in place by metal rods above the water reservoir. A short upwards section led to a 2-3 inch horizontal section, followed by the remainder of the sample which was bent downward. The important measurement for these samples was steady state performance during downward drainage. It is therefore acceptable to pre-wet such samples, saving time by eliminating the transient period.

3.4 Dye Experiments

Experiments were conducted in which the plies of a two ply sample strip were gently pulled apart at one end. One ply was dipped in water mixed with a non-substantive red dye, one in regular clear water. Water was allowed to wick to the top. The experiment was repeated with a sample from the same handsheet as before, however, the plies were switched. That is, if the softwood had previously been in the dyed water, it was now in the clear water. The concentration of dye in each ply was then inspected visually. The purpose of these experiments, depicted in Figure 3.4.1, was to determine from which ply the majority of water flow originated.

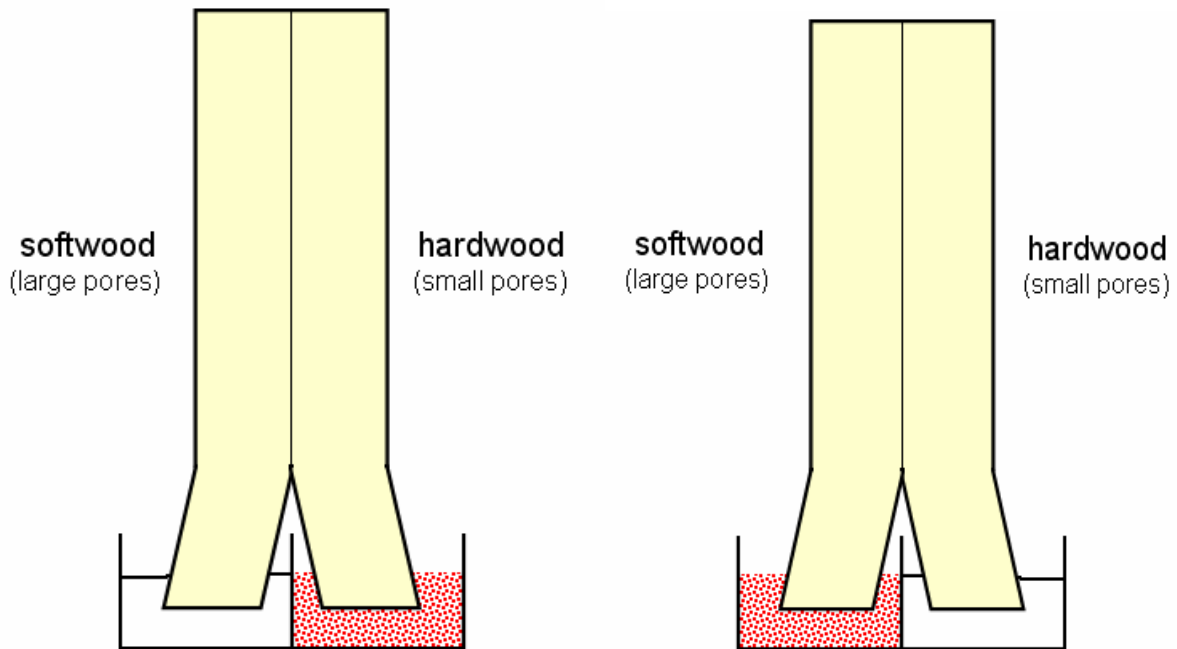


Figure 3.4.1 - Schematic of the dye experiments to determine direction of fluid transport

3.5 NMR Wicking Setup

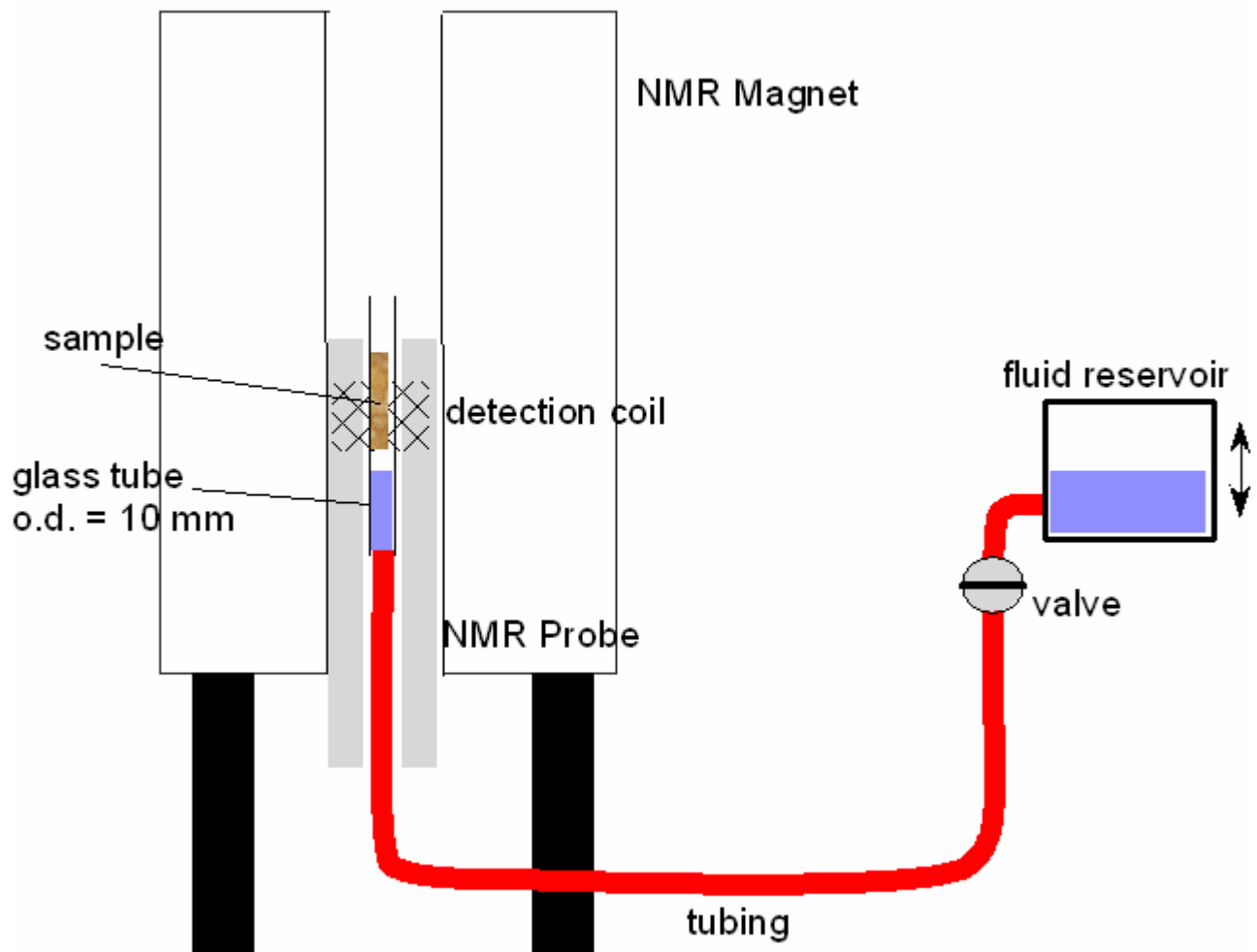


Figure 3.5.1 - Diagram of NMR experiment

A Bruker DSX 400 spectrometer was used to examine vertical wicking. The paper sample to be tested was placed in a thin glass tube which was then placed inside the NMR probe, as shown in Figure 3.5.1. A rubber tube connected the bottom of this glass tube to an external water reservoir. The height of the reservoir was adjusted so that the water level was about 2 inches below the NMR viewing area. Copper sulfate was added to this water to

decrease T_1 acquisition times, thereby allowing faster signal acquisition.¹⁴ Small pieces of plastic kept the sample from twisting or moving within the glass tube.

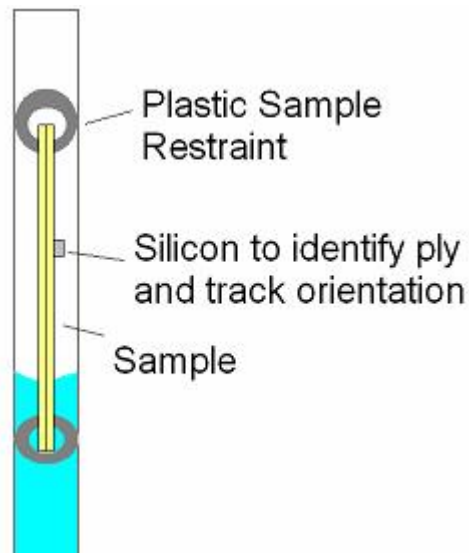


Figure 3.5.2 - Close-up of glass tube in NMR experiment.

For some experiments, small pieces of silicon rubber were glued to the hardwood ply of the sample to keep track of the sample's orientation prior to the beginning of the experiment. This step is necessary in order to properly align the sample for a sagittal or coronal view, and also to differentiate the softwood and hardwood plies of a two ply sample. The rubber pieces have a longer T_1 acquisition time than the water, affecting F_1 attenuation as described in equation 2.3.4. To detect them, the repetition time is upped to 200 ms. The repetition time is reduced back to 20 ms during wicking experiments, preventing the rubber from showing up.

Once the sample is in the tube, data acquisition is started and the reservoir valve is turned, raising the water level to the bottom of the sample.

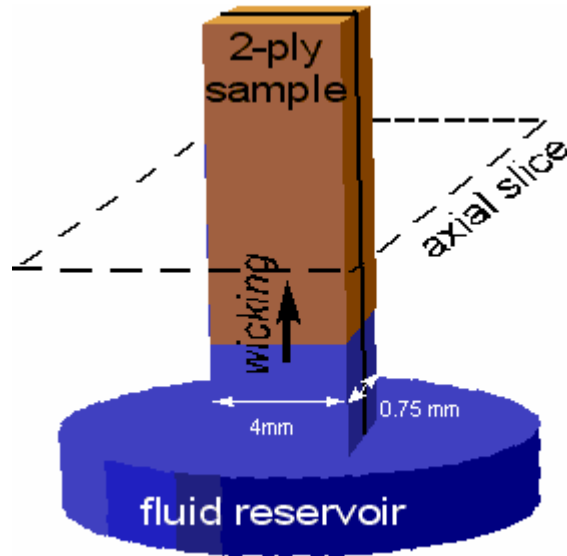


Figure 3.5.3 - Orientation of sample for NMR wicking experiments

The majority of NMR experiments took the form of axial views, a thin (2 mm) horizontal slice through the sample. As water enters the sample, it shows up in NMR images, with brightness proportional to the density of water. A new image is generated every six seconds, with a resolution of 128 by 128 pixels. A spin-echo technique was used. TR was set to 20 ms, TE to 5 ms.

The data from the NMR can be displayed in other ways.¹⁶ Using MATLAB, a program was written which takes the signal intensity across the thickness of the sample, and generates a graph of intensity vs. position vs. time. The MATLAB code is given in Appendix B.

CHAPTER 4: RESULTS AND DISCUSSION

4.1 Humidity Testing

Samples were tested inside an environmentally controlled chamber. However, it was discovered that simply maintaining the humidity of the chamber during tests was insufficient. It was also necessary to ensure that samples were equally conditioned, so that the initial moisture ratio of each paper sample did not vary.

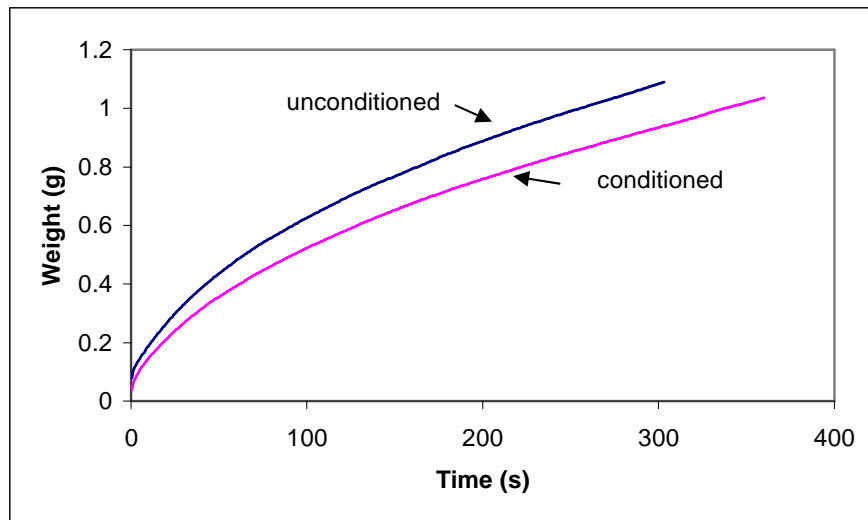


Figure 4.1.1 - Comparison of unconditioned sample and sample conditioned at 90% RH

Tests were done to confirm the necessity of conditioning samples for one hour prior to experiments (see Figure 4.1.1). One sample from a 2-ply handsheet was conditioned for an hour at 90% RH while another received no treatment. The unconditioned sample absorbed about 15% more water than the conditioned sample. This is because it is initially dryer, and also

because it will absorb more moisture from the air. Failure to condition all samples prior to beginning experiments will lead to exaggerated results for samples tested early, while later samples will have absorbed moisture from the air before being tested.

4.2 Gravimetric Wicking Results

Gravimetric wicking experiments formed the backbone of this investigation. These experiments were conducted to determine the amount of water wicked versus time for varied sample types, including multi-ply samples with dissimilar plies. These experiments measured weight wicked as well as height of capillary rise. The goal of the vertical wicking experiments was to investigate the existence of wicking enhancement in dissimilarly plied structures. The detailed results obtained using the electronic balance would allow for a closer investigation of how and why this enhancement exists.

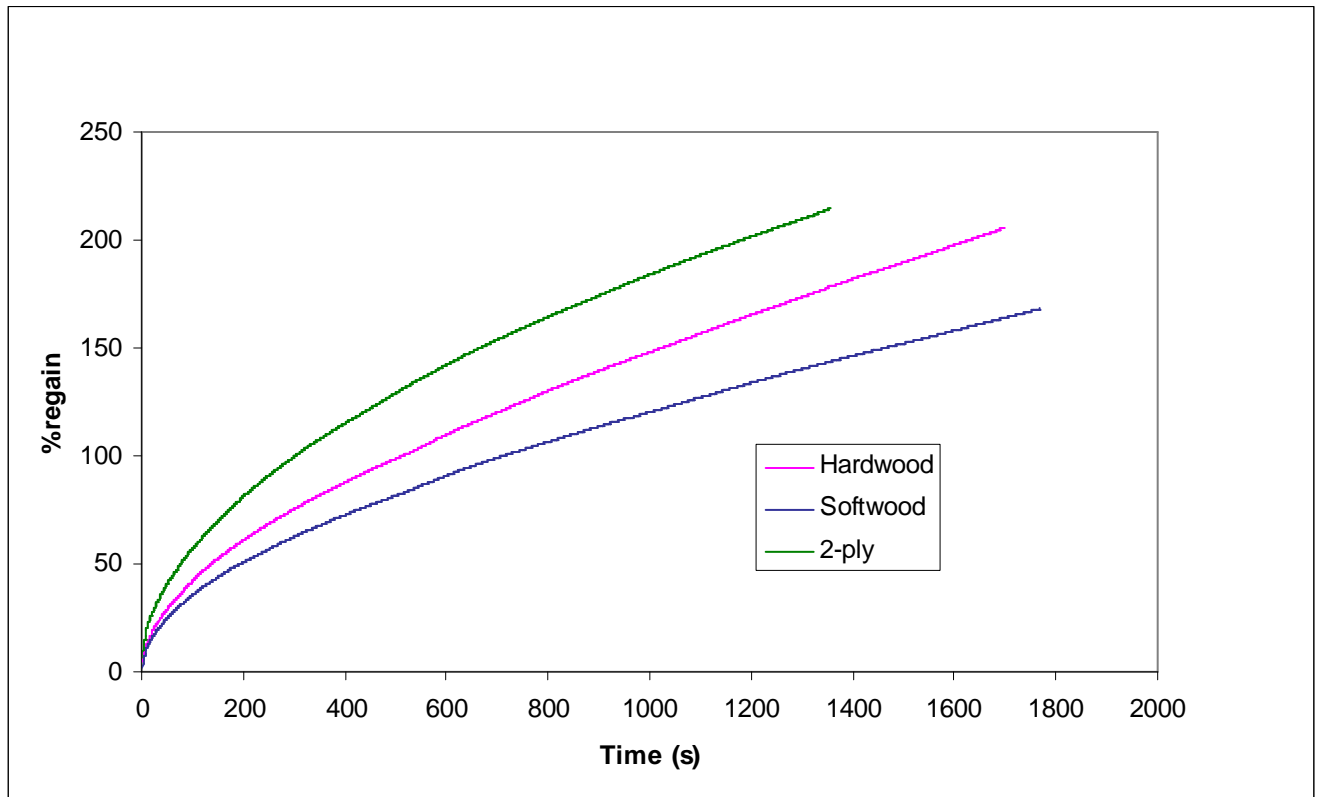


Figure 4.2.1 - % regain vs. time for varied sample type

Because of varying thickness and width of samples, results in Figure 4.2.1 are presented in terms of regain, defined as the weight of water divided by the initial weight of the sample. All samples were pressed at 20 psi unless specifically stated otherwise. The smaller pored hardwood material wicks more quickly than the softwood material, especially at higher heights. The two ply material wicks significantly more quickly than either of its component materials, with the most pronounced performance enhancement taking place at relatively low heights. Because data acquisition is not started until a second or two after the sample has made contact with water, the early stage (2-3 seconds) of wicking is missed. Since softwood leads during this stage (determined by visual inspection), these charts overemphasize the superiority of hardwood. Height versus time comparison (see Figure 4.2.2) shows a closer race, though in both cases the hardwood is clearly superior to softwood for most of the sample run.

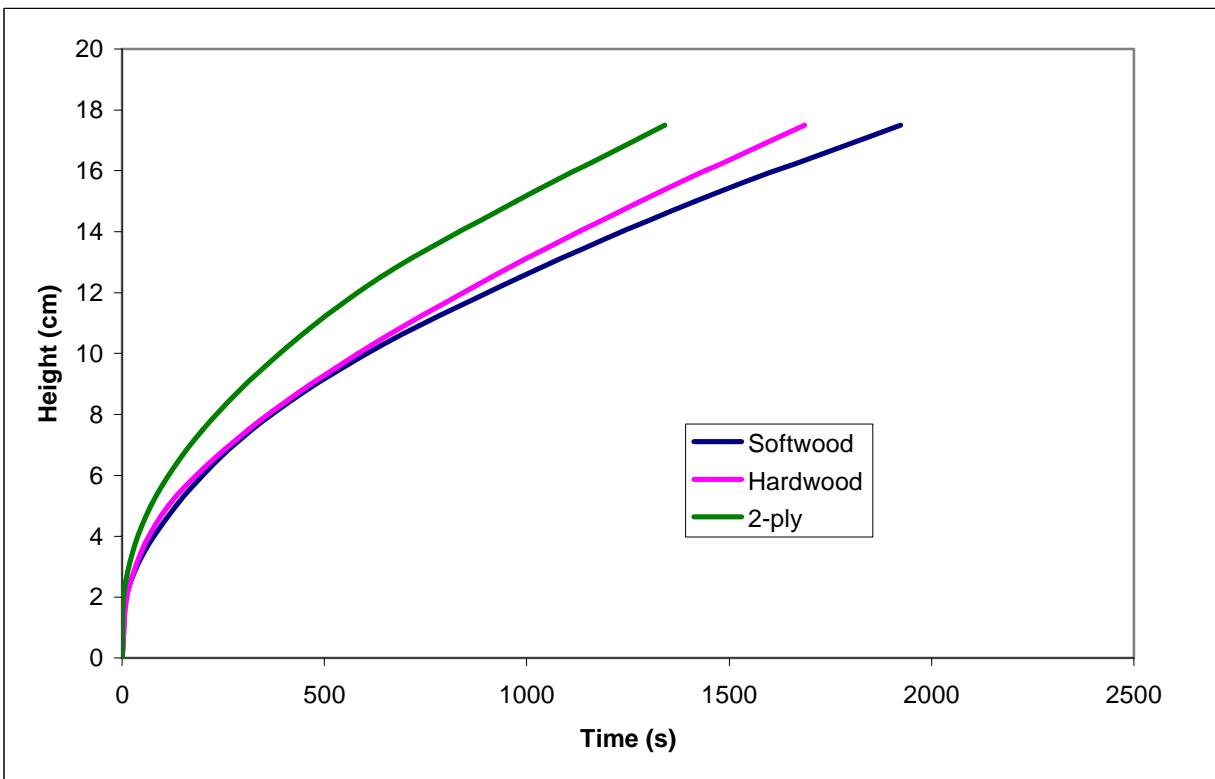


Figure 4.2.2 – Height vs. time for varied sample type

The two ply material exhibits the greatest enhancement early during wicking. The softwood ply is close to the hardwood in height early on, but lags later.

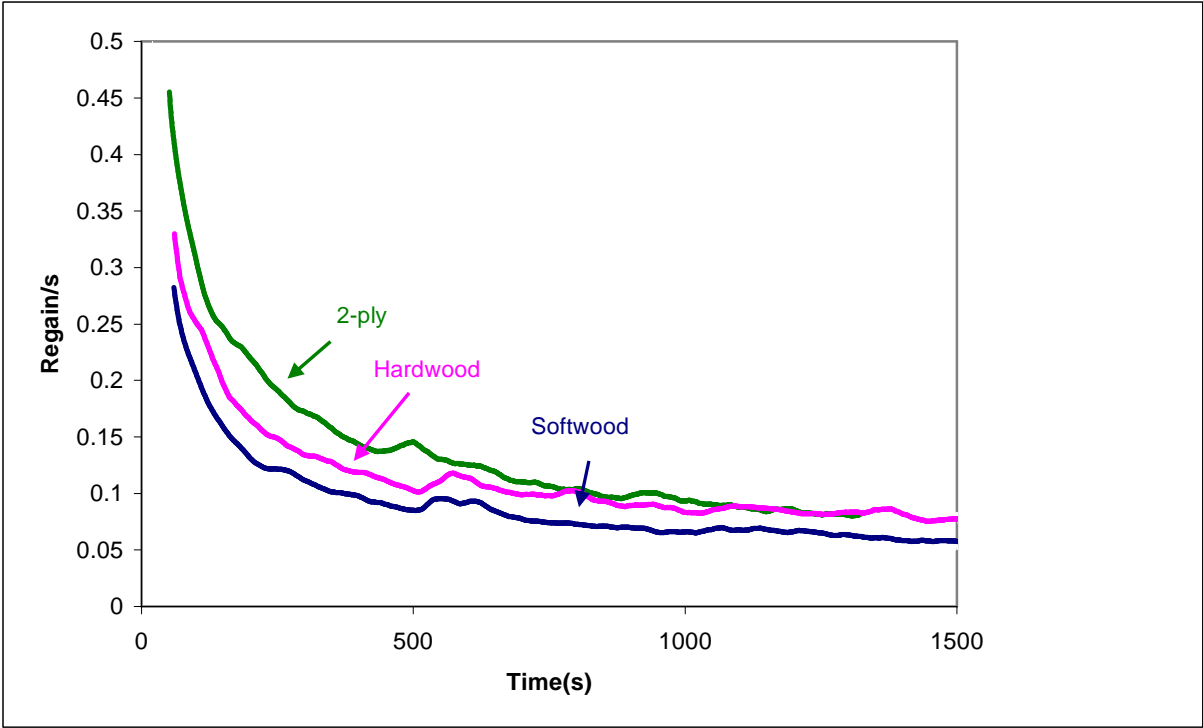


Figure 4.2.3 – Rate of water absorption for varied sample type

Comparing the rate of water absorption for the various samples (see Figure 4.2.3) clarifies the regain vs. time figure. The hardwood sample demonstrates clear superiority relative to the softwood, and does so for the entire experiment. The two ply sample is also superior to the softwood for the entire experiment. Compared to the hardwood, however, the two ply sample is

only temporarily superior. The curves gradually converge until they are roughly even. The multiply wicking enhancement diminishes. This may be because expansion is changing void sizes and permeabilities. It may also be because of the changes in the pressure as hydrostatic pressure increases. The enhancement does not entirely disappear, however, as even performance equal to the hardwood exceeds the hardwood/softwood average that would be expected if there was no fluid transport between plies.

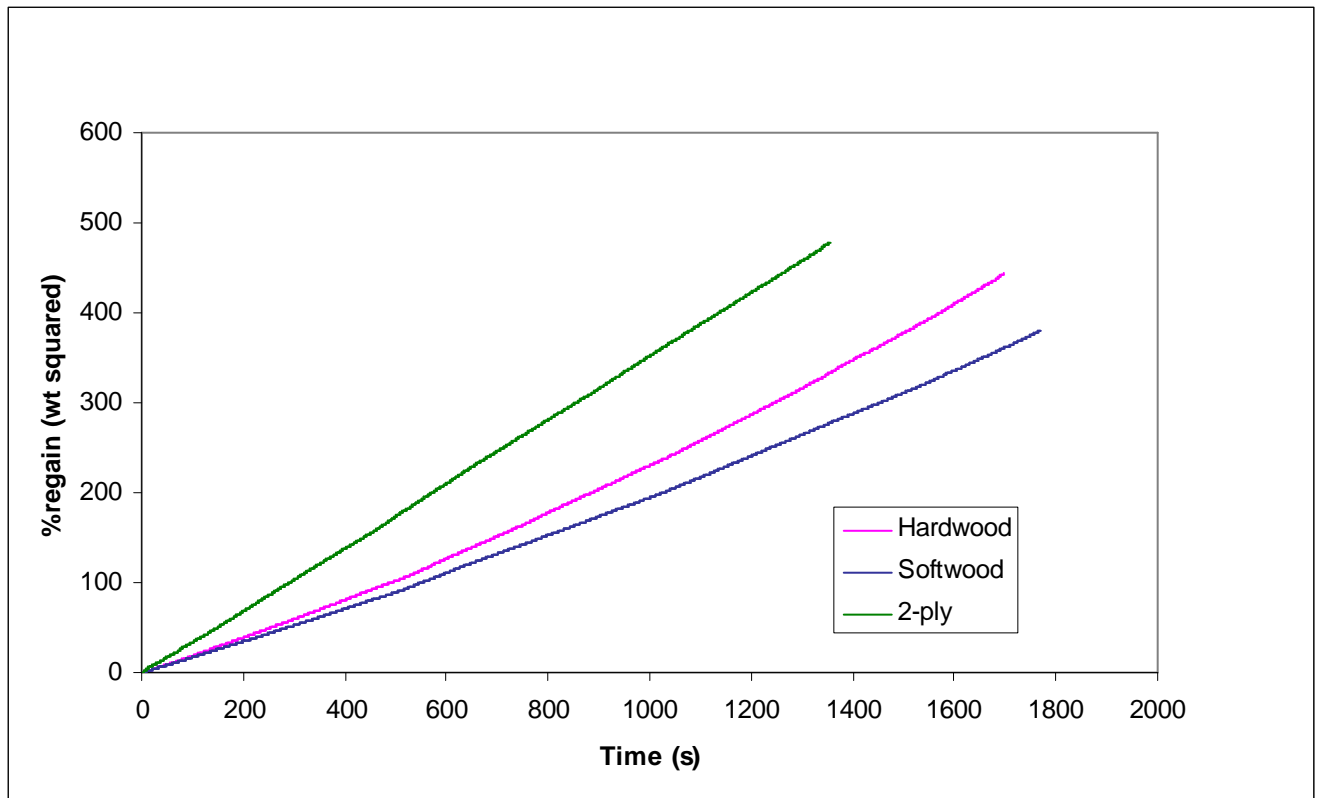


Figure 4.2.4 – Squared weight vs. time for varied sample type

It was predicted that there would be a linear relationship between time and the square of water

wicked, given by the equation

$$L^2 = \frac{2Kp_c t}{\varepsilon\mu} \quad (2.4.14)$$

As one can see in Figure 4.2.4, while somewhat close to linear, the relationship displays a slight upward curve. This is most likely due to the effect of bulk expansion. The volume of the sample increases following wetting, causing a greater amount of total absorption than would be found in a non-expanding medium. The curve occurs because initially the rate of vertical rise occurs quickly relative to outward expansion, so that the behavior is similar to that of a non-expanding material. As rise slows down, the expansion at lower levels continues, causing greater absorption than predicted by the equation. This is more pronounced in the softwood sample, displaying that the softwood sample expands to a greater extent. The 2-ply sample has the multi-ply enhancement factor providing greater absorption during the early period, and eventually tapering off. Two separate phenomena produce greater than expected wicking during both the early and late periods, so that the slope as a whole is straight but steep.

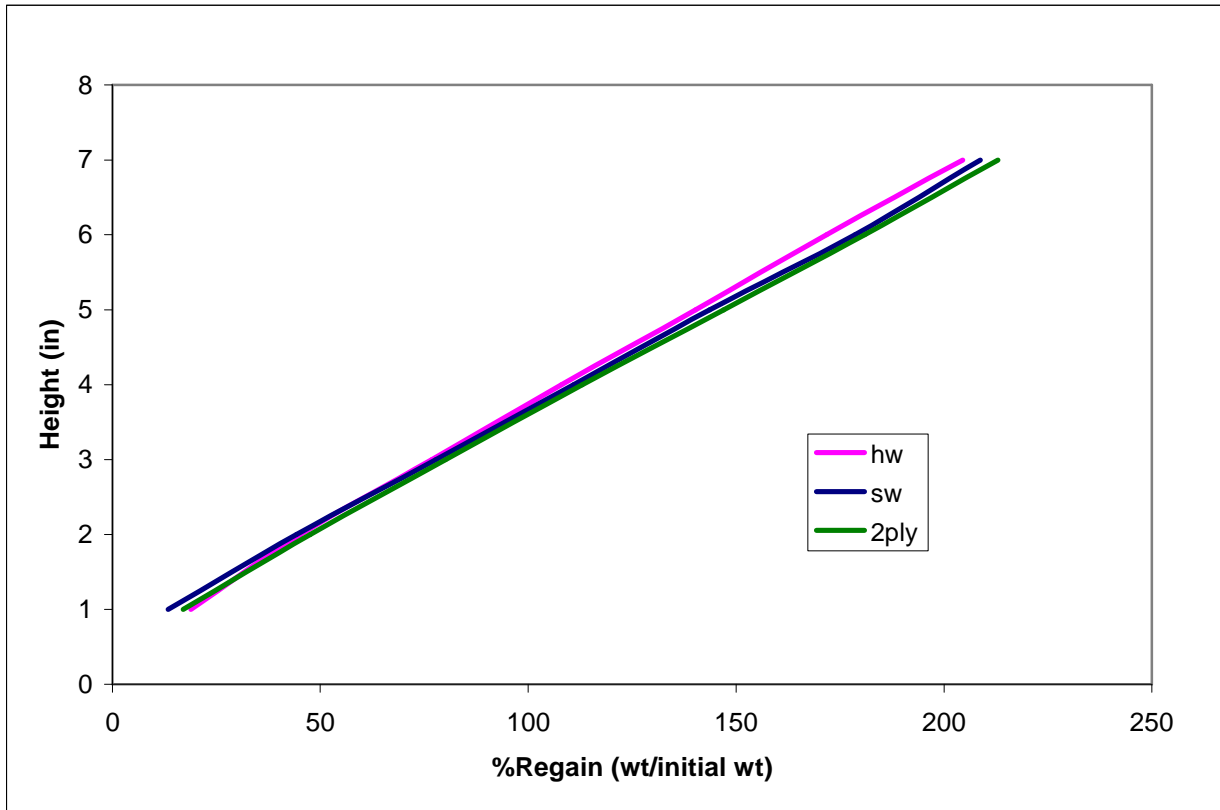


Figure 4.2.5 - % regain vs. height of wicking front

Figure 4.2.5 compares height versus weight data for the three sample types. The relatively straight line nature of the results is consistent with a fully saturated wicking front. This is the result you would get from say, capillary tubes which all share the same diameter. An array of differently sized vertical capillaries would see a gradual reduction in weight/ height as the larger pores fall behind the smaller pores¹¹. The largest pores would eventually stop transporting fluid entirely, when hydrostatic pressure equals capillary pressure. So this result demonstrates that paper, unlike textiles, does not behave in this fashion. It is not, however, possible to jump to the conclusion that wicking is fully saturated, and that paper is equivalent to capillary tubes whose diameter changes with height, like those discussed by Staples and Schaffer.¹²

A more detailed investigation of weight versus height was performed. The experiment

consisted of a sample being tested under the same conditions as the samples described above. Height was marked off to the inch. As soon as water reached the top of the sample, it was removed and cut into one inch segments. Each segment was then weighed separately. While the difficulties involved in precisely and quickly cutting wet paper introduced some error, the result (shown in Figure 4.2.6) is unmistakable.

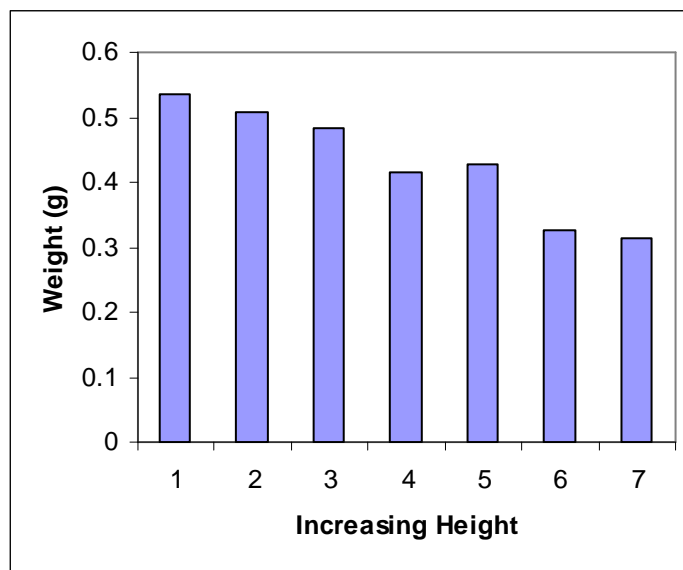


Figure 4.2.6 - Variation in weight of inch long segments, vs. height

A gradient clearly exists. However, it is not the kind of water density or “filling fraction” gradient found in textiles, or else the rise versus weight gain ratio would not be linear. The explanation instead falls to the bulk expansion of the paper sample. Paper’s chemical structure causes a weakening of fiber bonds and an increase in web volume, as well as swelling of the individual fibers. So the lower samples not only have a greater weight of water, but a greater volume. Volumetric expansion allows for the fully saturated condition to be true while at the same time allowing for variation in the weight of water at a given height. Observation via NMR

allows for this expansion to be documented and to some extent quantified.

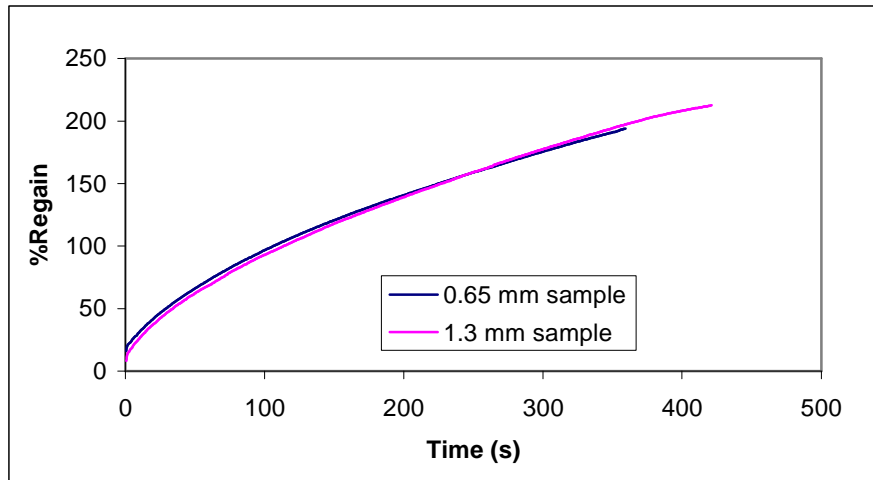


Figure 4.2.7 - Effect of sample thickness on regain

The effect of sample thickness was found to be negligible (see Figure 4.2.7). There was concern that the interfacial region might be playing a large role in the wicking process. To test this, thicker sheets were used so as to decrease the percentage of pores at the interface by increasing the number elsewhere. Little to no change in wicking performance was found. NMR images would later confirm that the interface region was not a major wicking conduit.

Additionally, there does not appear to be any advantage to fluid exchange from a thinner sample. This is reasonable, as the lateral distance between the centers of the two plies remains small relative to the length of the sample. Extreme increases in thickness will likely reduce fluid exchange.

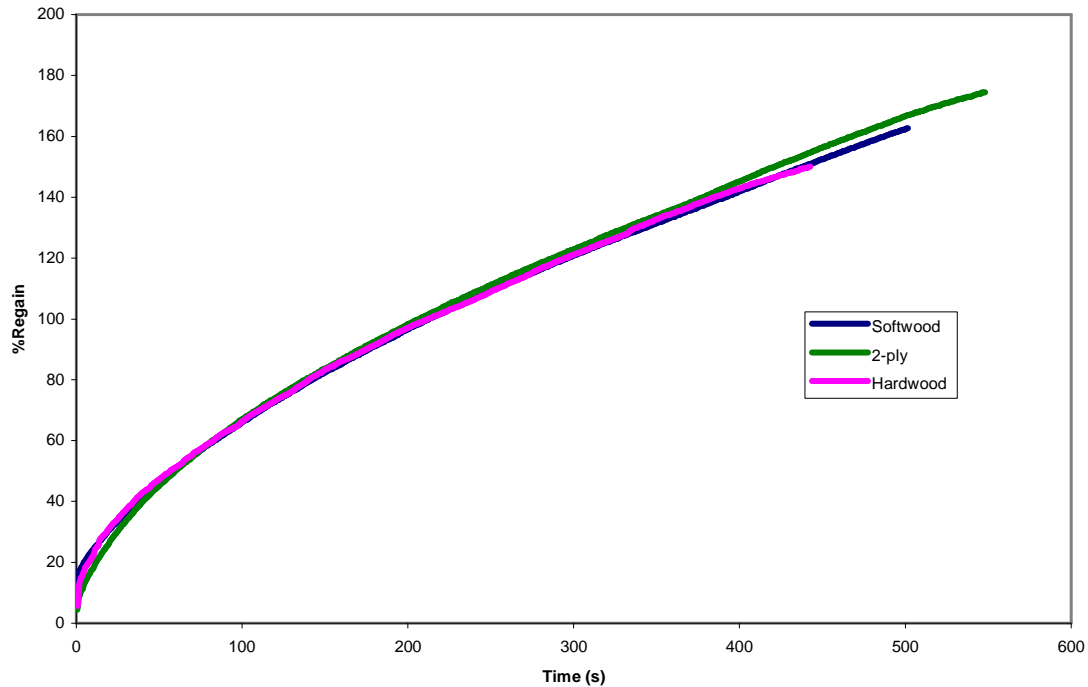


Figure 4.2.8 - Result of gravimetric wicking experiment with samples pressed at 45 psi

Highly pressed samples presented seemingly counter-intuitive results. The 2-ply sample sometimes displayed the worst performance, and in some sheets softwood out-performed hardwood. The clear advantages seen with the more lightly pressed samples did not appear (see Figure 4.2.8). The initial assumption was that heavier pressing would produce smaller pores, but that the ratio of pore sizes would not change. This assumption was not correct, as shown by porometry testing.

4.3 Porometry Results

Porometry tests, as described in Chapter 3.2, attempt to evaluate pore sizes comparing air flow through wet and dry samples. These experiments were performed in order to confirm the existence of pore size differences between hardwood and softwood at various pressing levels. They were not performed with the goal of establishing a meaningful quantitative estimate of pore sizes.

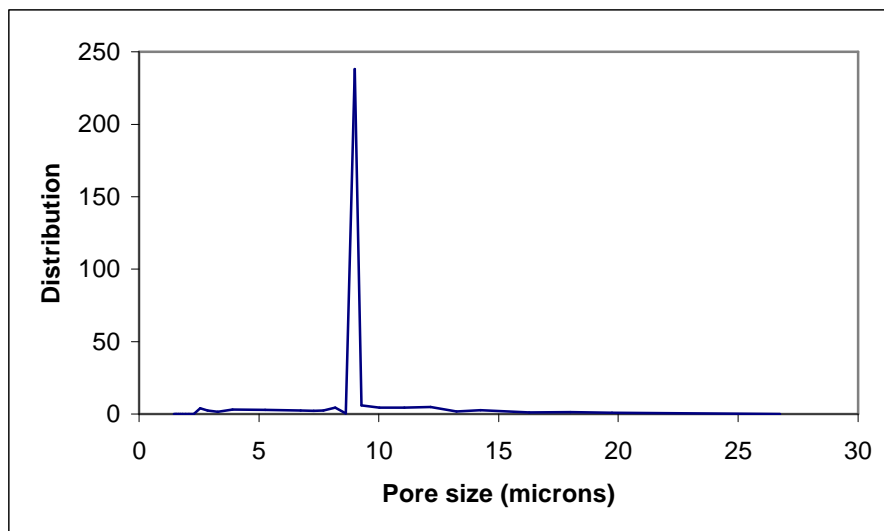


Figure 4.3.1 – Porometry test on softwood sample

The results of the porometry tests varied widely, with many large outliers among the data set. Softwood samples had a larger average pore size, both in the dry state and the wet state simulated via freeze drying. This is the expected result, and was found in 20 psi samples, shown in Figures 4.3.1 and 4.3.2. Noteworthy is that the pore distributions for most samples

show a single large spike, as opposed to say a gaussian curve, or a bimodal distribution. This is frequently caused by inadequacies in the software analyzing the flow, and large spikes are artifacts of the differentiation performed by the software. Drainage of small pores has a small effect on the total flow relative to the drainage of the largest pores, making them more difficult to detect. The method employed by the porometer does not account for pores whose size changes, as was shown in Figure 3.2.2 . In order for a pore to empty, the pressure difference must be sufficient to overcome the capillary pressure at the pores narrowest point.¹⁷ Relating flow to pore size will not give precise results for this kind of system. The pore structure cannot be approximated via parallel pores of varied diameter, but rather it must be treated via equivalent pore sizes¹².

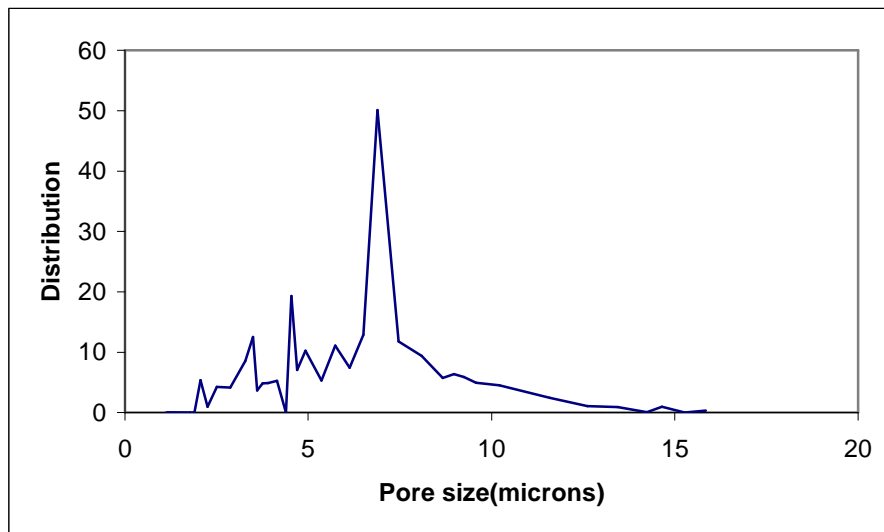


Figure 4.3.2 – Porometry test on hardwood sample

Samples pressed at more than 20 PSI showed a wide range of pore size results. In some

cases, the hardwood possessed larger pores than the softwood. In others, the pores were the same size. High press loads significantly altered differences in pore size distribution, explaining the erratic results of gravimetric wicking tests using such samples, such as those seen in Figure 4.2.8.

Table 4.3.1 - Average pore size (microns) at different pressing levels

	Hardwood	Softwood
20psi	6.4	8
45psi	4.7	4.5
80psi	4	4.2

4.4 Results of Dye Experiment

The experiment using dyed water was performed to determine the path of water flow. When the softwood ply was immersed in the dyed water (see Figure 4.4.1), and the hardwood in clear, both the hardwood and softwood plies showed significant amounts of dye. When the plies were reversed (see Figure 4.4.2), less coloration was visible, and the softwood ply was nearly untouched, especially at lower heights. This suggests that the bulk of the water being wicked originates in the softwood side. The primary direction of exchange is from softwood to hardwood. This is not universal, as some dye can be seen in the softwood at higher heights in the second experiment. This may simply be diffusion of the dye.

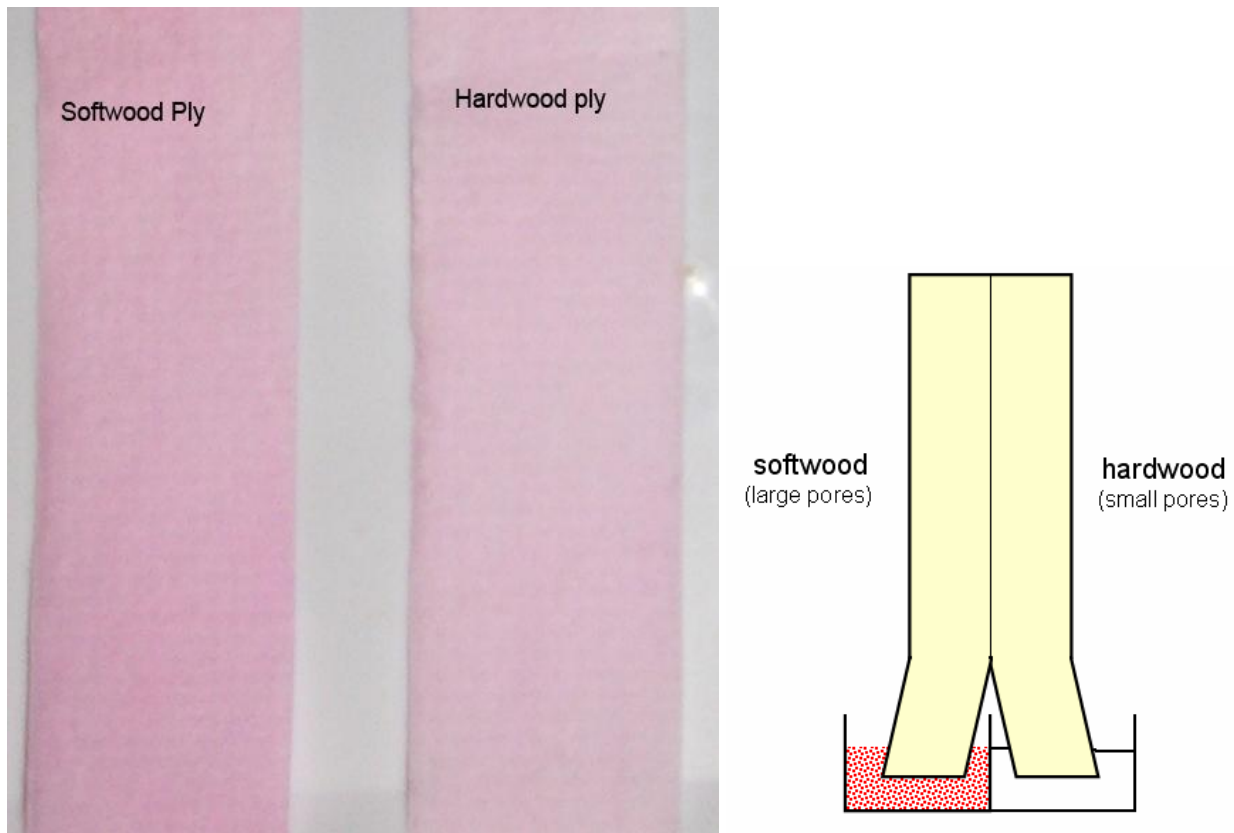


Figure 4.4.1 - Dye experiment result with softwood ply in dye

The conclusion to be drawn from these experiments is that the bulk of water wicked vertically initially comes from the softwood ply. This stands to reason, as the larger pores exhibit superior wicking at low heights. Conclusions can also be made on the direction of transport. Both plies contained significant amounts of dye when the softwood end was in the dyed water, but only the hardwood contained large amounts of dye when the hardwood was in the dyed water. This is consistent with water passing from the large pores of the softwood side to the smaller pores of the hardwood side. The capillary force on the hardwood side is higher, and the pressure difference drives this transfer. At higher heights, there seems to be a degree of equalization as the dye is more evenly distributed. This is likely because exchange from softwood to hardwood and back has occurred, producing uniformity. This exchange would occur as the water in the leading edge of the hardwood ply front wicks into the dryer softwood sample. This may occur because the saturated hardwood pores expand, removing their capillary pressure advantage over the dry softwood pores. Once the softwood sample is saturated, the once again smaller pores in the hardwood side will cause liquid to flow back towards the hardwood side. This is purely speculative. An even simpler explanation would be simply to attribute the transfer to diffusion of the dye.

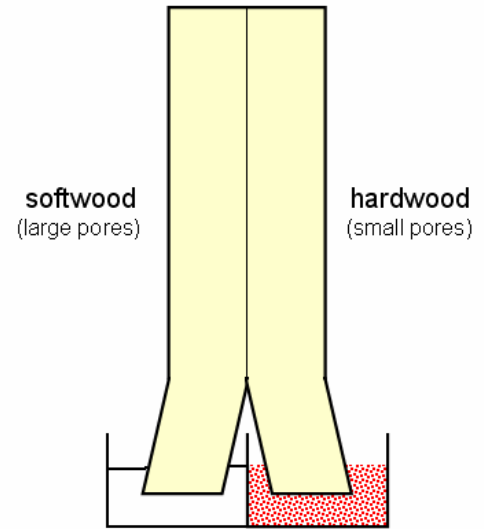
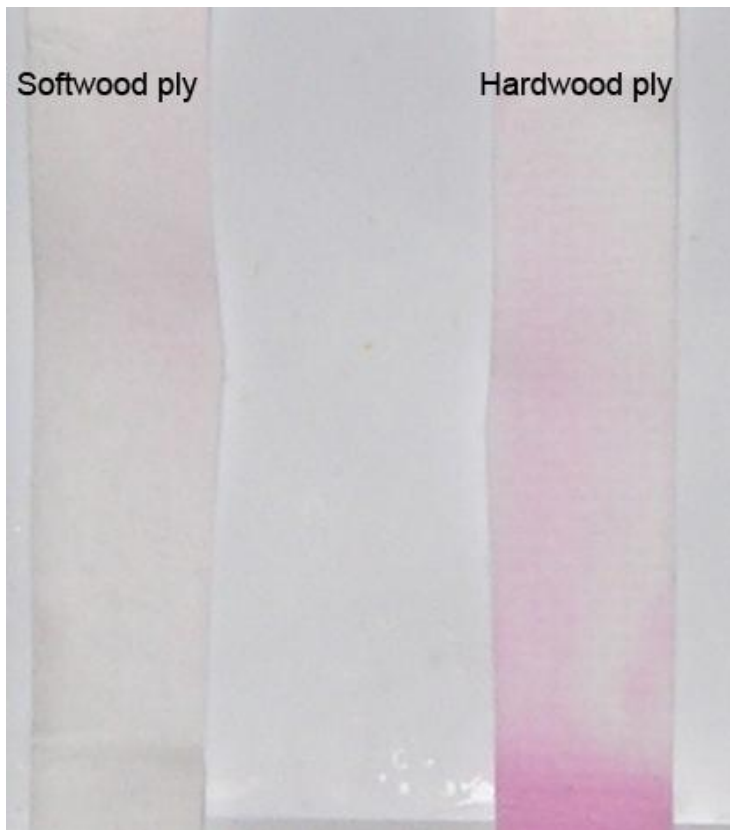


Figure 4.4.2 - Dye experiment result with hardwood ply in dye

4.5 NMR Wicking Results

NMR experiments were performed in order to determine which ply contained the leading edge of the wicking front, and also to evaluate the shape of this front. NMR tests also allowed observation of the process of bulk expansion during wicking, as well as the degree of saturation at various levels behind the wicking front.

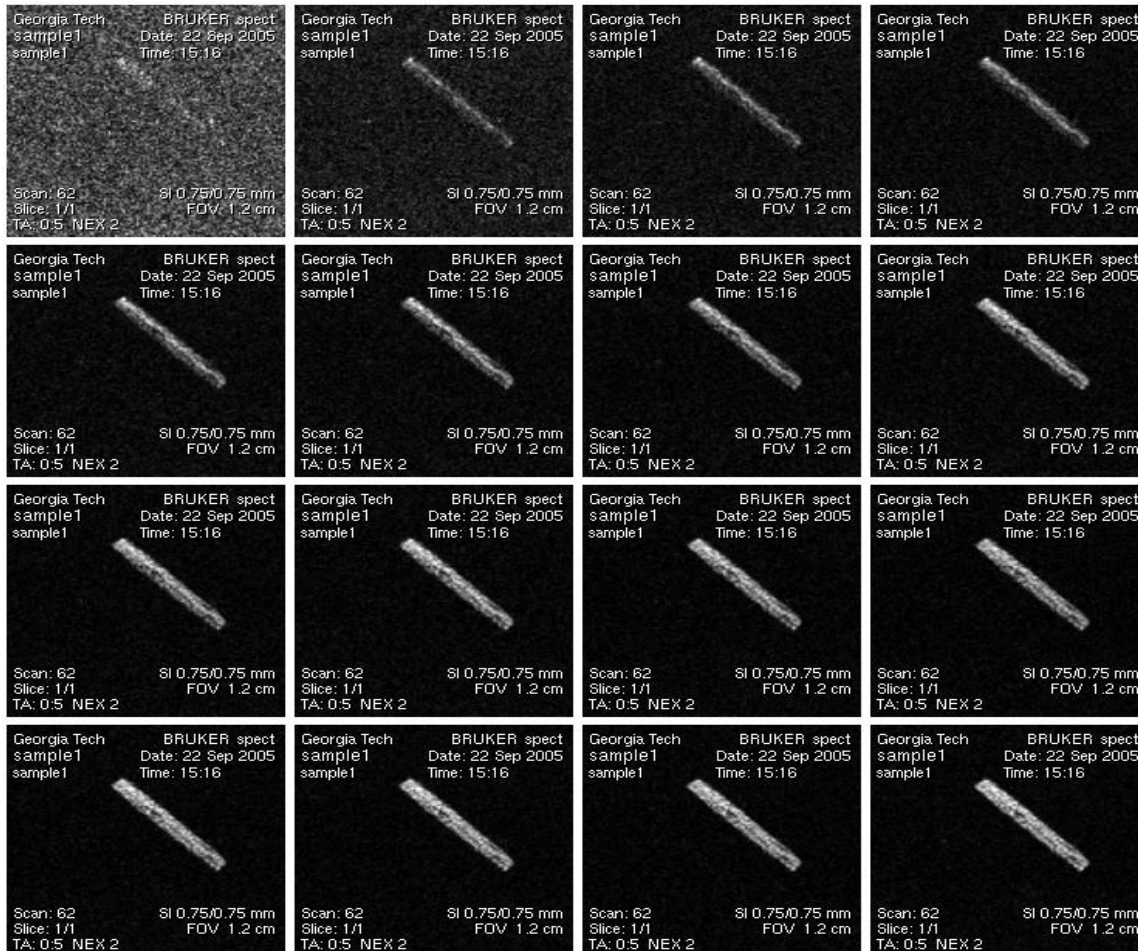


Figure 4.5.1 - Series of axial NMR images of a two ply sample. Hardwood side is up and to the right.

Figure 4.5.1 shows a slide show of images taken during NMR, capturing the early period of

wicking. Increasing brightness signifies greater water uptake. The interface between the two plies can be seen, as can the gradual expansion of the sample.

Looking more closely, the shape of the wicking front can be observed, as shown in Figures 4.5.2-4.5.5. In every experiment, water is first seen appearing on the hardwood side of the sample.

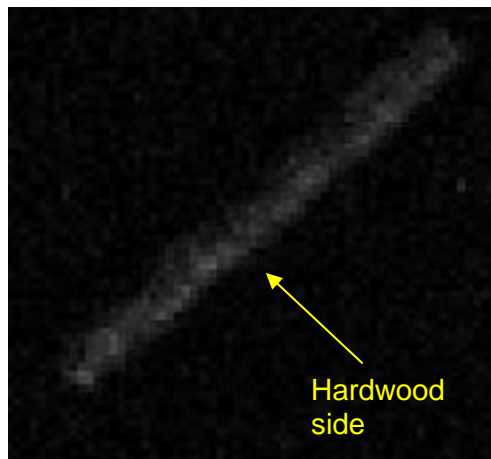


Figure 4.5.2 - NMR image of two ply sample at $t = 72$ s

Less than 10 seconds later, water can be seen in the softwood side.

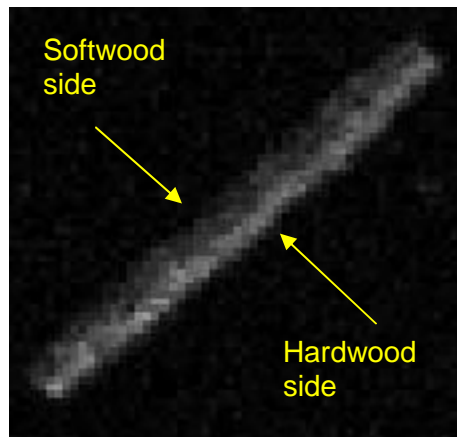


Figure 4.5.3 - NMR image of two ply sample at $t = 78$ s

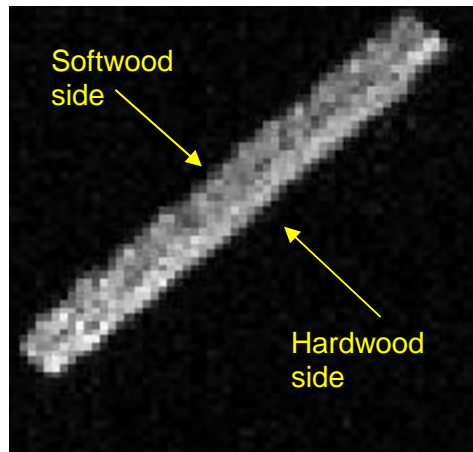


Figure 4.5.4 - NMR image of two ply sample at $t = 144$ seconds

The two plies become more heavily saturated, followed by expansion of the paper structure to as much as 125% of its initial thickness. Slightly more expansion seems to take place on the softwood side of the sample. A concentration gap of sorts is visible in between the two plies late in the process. This region does not saturate as fully as the area within the plies.

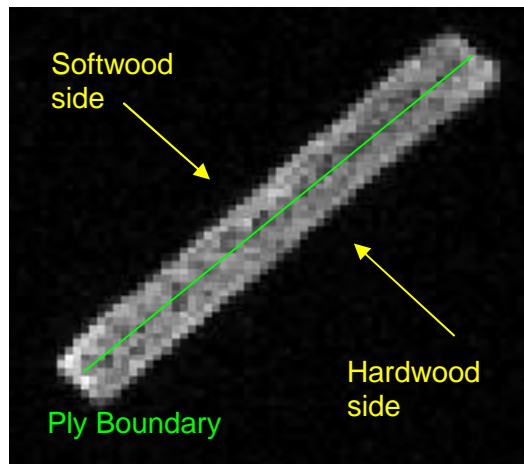


Figure 4.5.5 - NMR image of two ply sample at $t = 552$ seconds

At higher heights, this process happens more slowly, with a greater lag between the appearance of water in the hardwood ply and the softwood ply. This is consistent with theory, as the smaller pore size in the hardwood ply produces a greater capillary pressure, causing a gradually increasing lead over the softwood ply. This is also consistent with the results of bulk wicking, in which hardwood's wicking advantage increased with increased height. Cross referencing data on the speed of vertical rise (from gravimetric experiments) with the NMR data, it is found that this lead is never more than about 2 millimeters. However, the softwood side does seem to take significantly longer to fill to its maximum expansion compared to the hardwood.

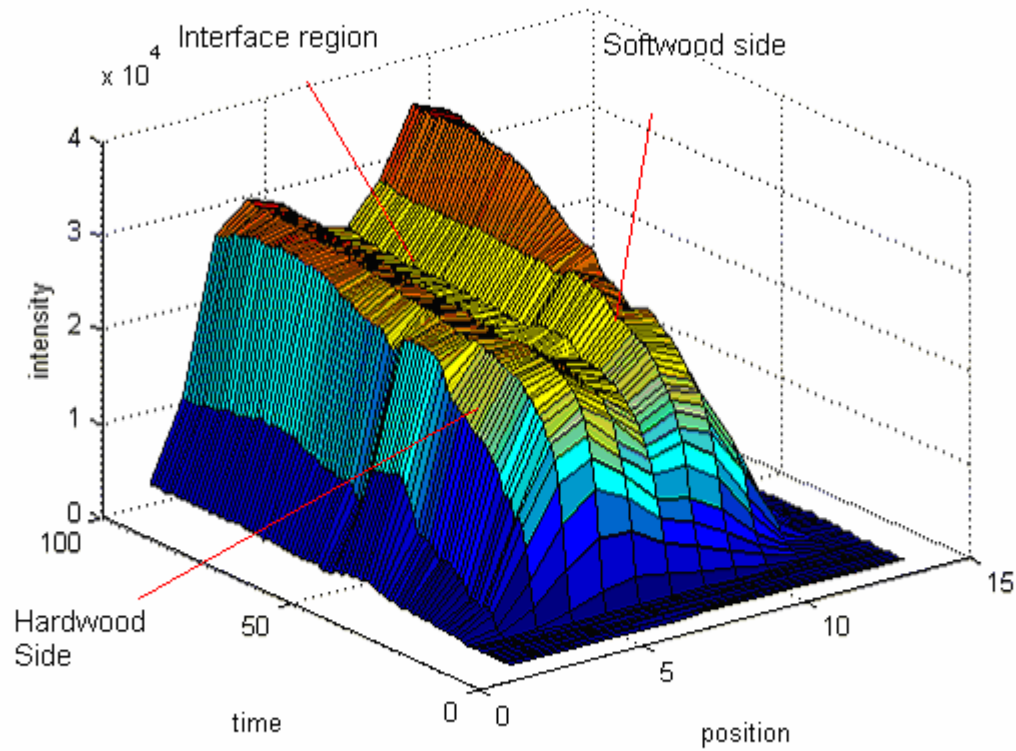


Figure 4.5.6 - 3-D graph of NMR wicking experiment

The three-dimensional graph in Figure 4.5.6 shows this behavior. The initial wicking occurs in the hardwood side to the left of the graph, followed very closely by the softwood on the right. The “valley” between the two is clearly visible, representing the inter-ply region. The softwood side, which has larger pores, reaches a higher final intensity. The “peak” of the softwood side shifts outward somewhat as a result of expansion. Resolution limitations can blur the distinction between increasing water density and volumetric expansion, especially when the data are converted into graph form.

4.6 Downward Gravimetric Tests

Downward wicking and drainage tests were performed primarily with the goal of determining permeability and capillary pressure of the various sample types. Miller proposed a method for determining these parameters from downward wicking tests. An alternative method instead uses downward drainage tests, which look at a fully wetted sample. Downward wicking is flow in a downward direction through an initially dry sample. Drainage is downward flow through a wet sample. A fully wetted sample has no meniscus and no capillary pressure. Drainage, provided the sample is fully saturated, is controlled only by the permeability of the sample and the hydrostatic pressure.

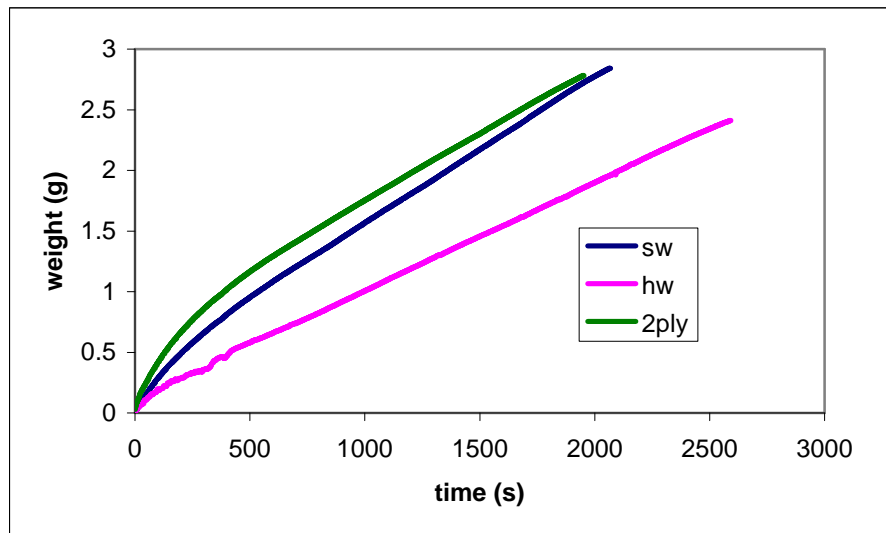


Figure 4.6.1- Results of upward, horizontal, and then downward wicking tests.

Downward drainage tests (see Figure 4.6.1), following a transient vertical and horizontal period, quickly reach steady state, as predicted earlier. Zeroing the results to show only the fully

saturated region gives constant steady-state drainage rates (see Figure 4.6.2).

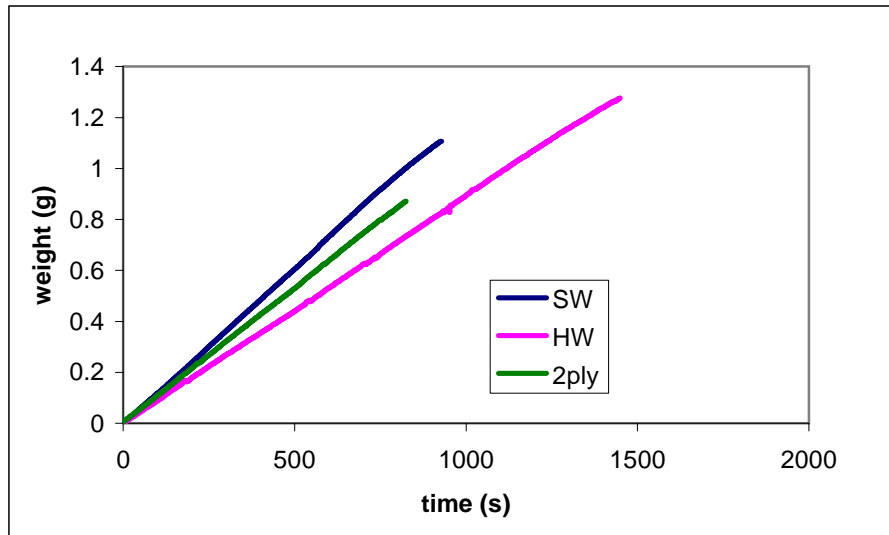


Figure 4.6.2 - Steady-state downward drainage results

It can be theorized that the flow per centimeter of thickness is constant. The slope for the two ply material would then be the average of the hardwood and softwood slopes, as the two plies are of the same thickness. The actual slopes, adjusted for dimensional variations, are given in Table 4.6.1.

Table 4.6.1 - Drainage flow rates for varied sample types.

Softwood	Hardwood	2-ply	Average of Softwood and Hardwood
1.201 mg/sec	0.889 mg/sec	1.057 mg/sec	1.045 mg/sec

There is no significant enhancement for the two-ply; the slight increase over the theoretical value may be attributable to gaps in the interfacial region. In any case, the phenomenon producing two-ply superiority during vertical upward wicking is clearly not present here.

Any attempt to model wicking behavior is going to require knowledge of the factors determining the behavior of each ply. More specifically, capillary pressure and permeability must be determined. Determining these directly is problematic, but they can be back calculated through observation of downward and horizontal flow rates. Miller gives various equations for doing so, (2.4.12-2.4.17). In practice, however, these equations are problematic.

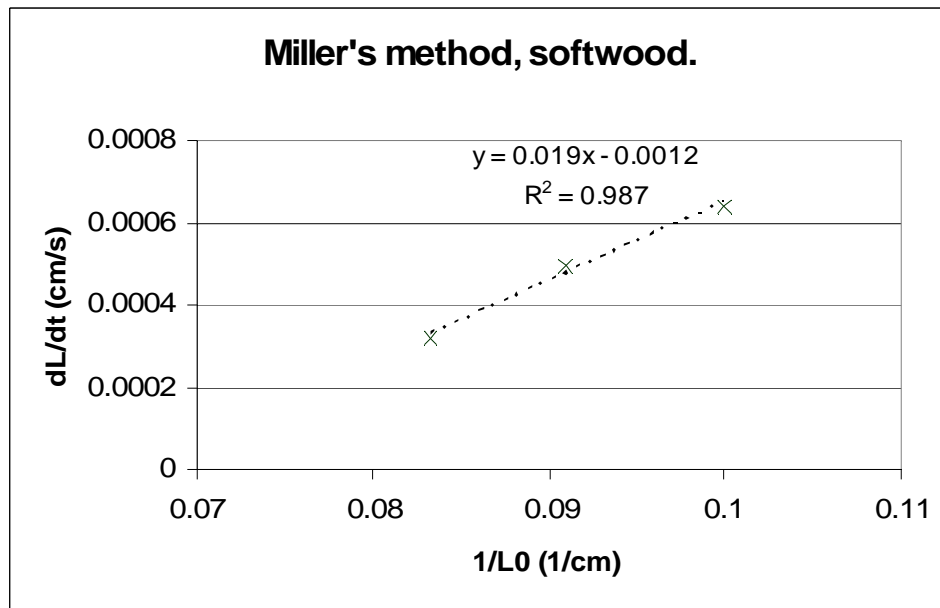


Figure 4.6.3 - Results of attempting to use Miller's method to determine permeability and capillary pressure

Miller's method relies on the fact that if the length of the vertical section of a downward wicking experiment is altered, the flow rate will drop proportionally.⁴ Because it is proportional, the capillary length (and capillary pressure) can be calculated, leaving permeability as the only unknown value. The line relating flow rate to L_0 is displayed above. According to theory, the slope and y-intercept will provide the necessary data to determine permeability and capillary pressure. In practice (see Figure 4.6.3), the y-intercept is negative, which produces nonsensical results of negative capillary pressure. It should be noted that the experimental setup used does not exactly match that used by Miller. The setup here had a vertical and a horizontal section, rather than a diagonal section. This was treated as equivalent to a diagonal with the same total length and the same ratio of vertical to horizontal displacement.

It is possible that the bulk expansion behavior of paper is at least partially responsible for the failure of Miller's method in this case. Miller's method assumes an unchanging porous medium, and the change in pore size and volume during the wicking process may have thrown off the results.

Instead, a drainage experiment was used. The sample was allowed to saturate completely, and enter a steady state with water dripping from the end of the sample.

The permeability was determined using equations 2.4.1 and 2.4.2, repeated here

$$Q = (zw)u \quad (2.4.1)$$

$$u = \frac{K\rho g}{\mu} \frac{L}{L_D} \quad (2.4.2)$$

The flow Q was obtained from the steady state drainage experiment. Viscosity and density of water are known, so permeability can be solved for. Results are given in Table 4.6.2.

Table 4.6.2 - Calculated permeability values for varied sample types.

	Softwood	Hardwood	2-ply
Flow (mg/s)	1.201	.889	1.057
Width (cm)	2.5	2.5	2.5
Wet Thickness (mm)	0.7425	0.74	0.76
Dry Thickness (mm)	0.65	0.65	0.66
Void Fraction (wet)	0.75	0.75	-
L (cm)	20	20	20
L _D (cm)	13	13	13
K (cm ²)	1.02*10 ⁻⁹ cm ²	7.5*10 ⁻¹⁰	8.9*10 ⁻¹⁰

As opposed to Miller's method, which attempts to calculate capillary pressure and permeability in a single experiment, this method only determines permeability. Full saturation means there is no wicking front, no meniscus, and henceforth no capillary pressure. Once the permeability is determined, capillary pressure is determined from Darcy's law, using upward wicking data from the same handsheet. Results are given in Table 4.6.3

$$p_c = \frac{L^2}{t} \frac{\varepsilon\mu}{2K} \quad (2.4.17)$$

Table 4.6.3 - Calculated capillary pressure and permeability. The 2-ply capillary pressure is a purely theoretical value, indicating the pressure which would produce the observed results for a single-ply sample with the same permeability.

	$L/t^{1/2}$	P_c (kPa)	K (cm ²)
Softwood	0.398	58	1.02*10 ⁻⁹
Hardwood	0.414	88	7.5*10 ⁻¹⁰
2-ply	0.498	102	8.9*10 ⁻¹⁰

Void fraction was calculated to be approximately 0.75 for both hardwood and softwood. This was done by comparing the wet and dry weight of samples, assuming full saturation. Since the densities of water and cellulose are known, the volume of water and cellulose can be calculated, and the ratio of water volume to total volume is equal to the void fraction.

$$\varepsilon = \frac{\frac{m_{wet} - m_{dry}}{\rho}}{\frac{m_{wet} - m_{dry}}{\rho} + \frac{m_{dry}}{\rho_{cell}}} \quad (4.6.1)$$

Using the P_c and K results and comparing to the results of vertical wicking experiments shows good agreement.

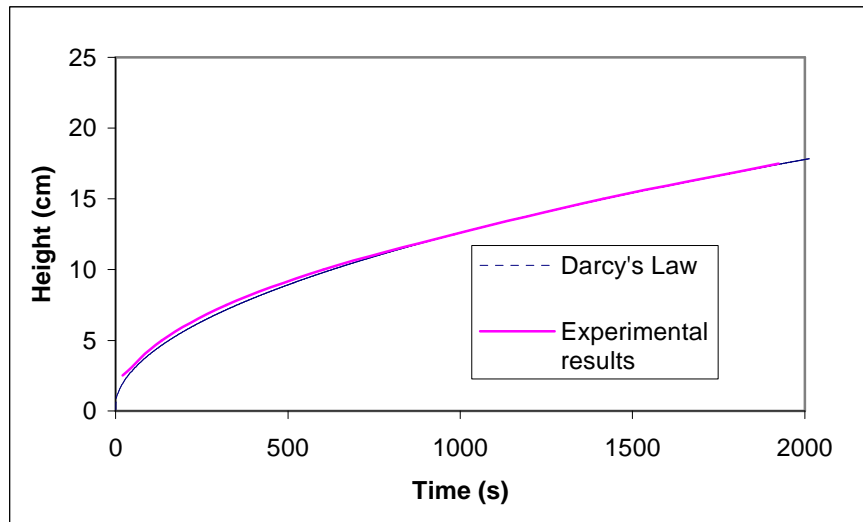


Figure 4.6.4 - Comparison of calculated and actual results for softwood sample

The result (see Figures 4.6.4 and 4.6.5) is not in itself remarkable, as these are the same experiments from which these variables were derived.

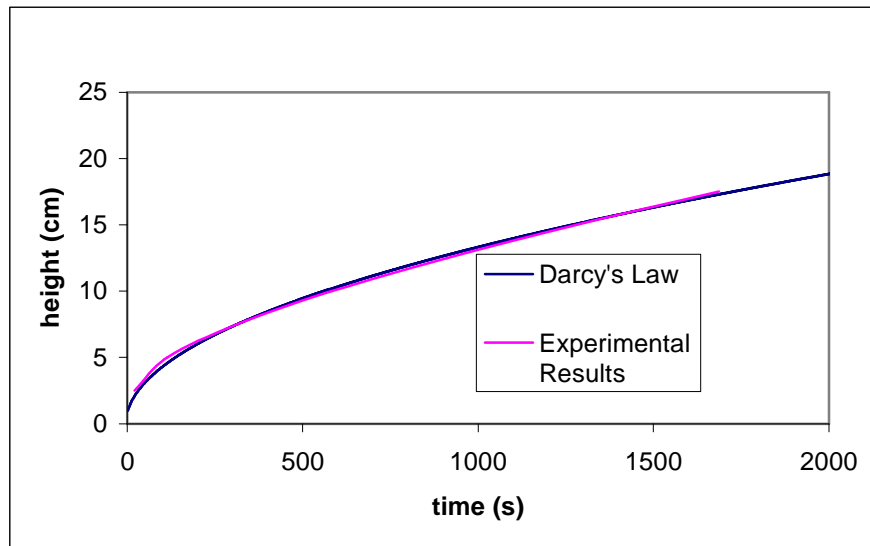


Figure 4.6.5 - Comparison of calculated and actual results for hardwood sample

The working theory for the mechanism of multi-ply wicking enhancement is that the bulk of liquid transport flow passes through the more permeable large pored ply, while the driving force is provided by the higher capillary pressure of the small pored ply. A test of this hypothesis would be to calculate the results of a sample with the capillary pressure of hardwood and the permeability of softwood.

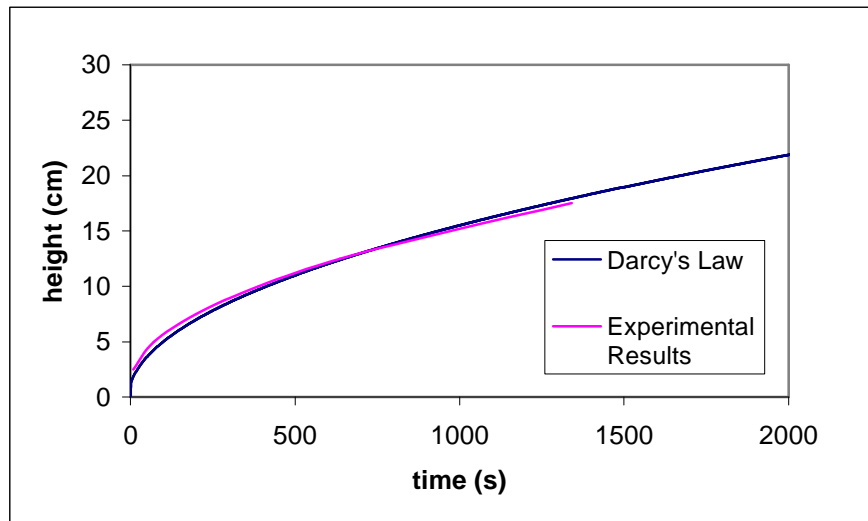


Figure 4.6.6 Comparison of calculated and actual results for 2-ply sample

The results (see Figure 4.6.6) match closely. This reinforces the results of the dye experiment, which implied that the bulk of lateral transport occurs from the softwood ply towards the hardwood ply. The leading edge of the wicking front is in the smaller pored hardwood ply. The likely path of a given fluid volume is upward through the softwood ply until it nears the leading edge, at which point it transfers laterally to the hardwood side.

CHAPTER 5: CONCLUSIONS

The goal of this investigation was to determine if and how multi-ply paper structures of dissimilar plies produce enhanced wicking performance. Through a combination of experimental methods, an accurate picture of the behavior of fluid in these structures was assembled.

- Two-ply materials with plies of different pore structure can offer wicking performance in excess of either component ply. This enhancement is most noticeable early in the wicking process, and gradually diminishes.
- Larger pore sizes produce higher permeability and lower capillary pressure. Smaller pores are superior except very early in the wicking process.
- In the two-ply material, the leading edge of the wicking front can be found in the material with smaller pores.
- The majority of liquid is initially drawn from the larger pored material, then transferred to the smaller pored material.

CHAPTER 6: FUTURE WORK

This investigation is by no means comprehensive, and there remains much to be determined regarding multi-ply wicking.

Basic improvements to the experimental procedure would include a more precisely controlled method of sample preparation and pressing, to ensure more uniformity of samples of the same type. Modification to the procedure to obtain more accurate data for wicking at very low heights would also be useful.

In this investigation, the effect of paper web expansion during wicking played a significant role. The significance of this expansion on the vertical wicking rate, and the variation of water weight and thickness with height are important questions, but perhaps best investigated separately. The use of artificial non-wovens with physical structure similar to paper, but non-swelling, would allow for wicking experiments without the pore size variation caused by paper web expansion. Alternately, rigid porous plates would provide a medium with completely unchanging pores.

Wicking in multi-ply structures of differing pore sizes may also be investigated using engineered fabrics of known physical dimensions and uniform pore sizes, as opposed to the much less predictable paper structure. Such experiments would have the advantage that precise computer modeling could be performed and compared to experimental results.

An important eventual step in this area would be to identify the effect of various factors (pore size distribution, thickness, etc.) on the degree of wicking enhancement. Optimization of wicking enhancement could then be attempted. Once the variables controlling enhancement are known, these might be tweaked to design paper samples that meet specific criteria for wicking performance.

Appendix A: Modeling

It was hoped that a model to explain wicking enhancement could be developed. This appendix is a one dimensional analytical model of wicking in a two ply material. Flow between plies is modeled using fluid resistance. It neglects many effects observed experimentally, such as saturation and expansion gradients. This model does not accurately predict the two-ply enhancement factor which was the focus of the experiment, and is therefore presented as an appendix. It is included for the sake of completeness and in the hope that it will be of use to future researchers attempting to assemble a more complex and accurate model.

The simplest method with which to model wicking is to assume fully saturated flow. All pores behind the wicking front are assumed to be full. A further simplifying assumption is to assume that there is no bulk expansion. The capillary pressure, permeability, and other parameters dependent on pore size thus remain constant. The basis for this model is Darcy's law

$$\frac{dL}{dt} = \frac{K}{\varepsilon\mu L} P_c \quad (\text{A.1})$$

For simplicity, we neglect the hydrostatic pressure

For multi-ply wicking, Darcy's law is applied to vertical transport in both plies, as well as the lateral transport between them. This gives a continuity equation for each ply.

$$\delta_1 \frac{dV_1}{dx} = -Q_{12} \quad (\text{A.2})$$

$$\delta_2 \frac{dV_2}{dx} = Q_{12} \quad (\text{A.3})$$

Where Q is the superficial velocity of the lateral transport.

$$Q_{12}(x) \approx \frac{p_1^{(x)} - p_2^{(x)}}{\mu R} \quad (\text{A.4})$$

R is a resistance term obtained from the weighted average of the permeability of each ply. Note that z directional permeability may not necessarily equal in plane permeability.

$$R \approx \frac{\delta_1}{2K_{1z}} + \frac{\delta_2}{2K_{2z}} \quad (\text{A.5})$$

The in plane velocities are given by Darcy's law equations:

$$V_1 = \frac{-K_1}{\mu} \frac{dp_1}{dx} \quad (\text{A.6})$$

$$V_2 = \frac{-K_2}{\mu} \frac{dp_2}{dx} \quad (\text{A.7})$$

with the boundary conditions

$$\begin{aligned} p_1(0) &= 0 \\ p_1(l) &= -P_{c1} \end{aligned} \quad (\text{A.8})$$

$$\begin{aligned} p_2(0) &= 0 \\ p_2(l) &= -P_{c2} \end{aligned} \quad (\text{A.9})$$

at the wicking front, that is, $x = L(t)$ (assumed to be the same in each ply)

$$V_1(t) = \varepsilon_1 \frac{dL}{dt} \quad (\text{A.10})$$

$$V_2(t) = \varepsilon_2 \frac{dL}{dt} \quad (\text{A.11})$$

Inserting the equations for superficial velocity into the continuity equations gives

$$\frac{-\delta_1 K_1}{\mu} \frac{d^2 p_1}{dx^2} = -\frac{(p_1 - p_2)}{\mu R} \quad (\text{A.12})$$

$$\frac{-\delta_2 K_2}{\mu} \frac{d^2 p_2}{dx^2} = \frac{(p_1 - p_2)}{\mu R} \quad (\text{A.13})$$

$$\frac{d^2 p_1}{dx^2} = \frac{1}{\delta_1 K_1 R} (p_1 - p_2) \quad (\text{A.14})$$

$$\frac{d^2 p_2}{dx^2} = -\frac{1}{\delta_2 K_2 R} (p_1 - p_2) \quad (\text{A.15})$$

Note that

$$\delta_1 K_1 \frac{d^2 p_1}{dx^2} + \delta_2 K_2 \frac{d^2 p_2}{dx^2} = 0 \quad (\text{A.16})$$

Introducing a new variable

$$\tilde{p} = \delta_1 K_1 p_1 + \delta_2 K_2 p_2 \quad (\text{A.17})$$

and substitute

$$\frac{d^2 \tilde{p}}{dx^2} = 0 \quad (\text{A.18})$$

Applying the boundary conditions,

$$\tilde{p}(0) = 0 \quad (\text{A.19})$$

$$\tilde{p}(L) = -(\delta_1 K_1 P_{c1} + \delta_2 K_2 P_{c2}) \quad (\text{A.20})$$

The solution is of the form

$$\tilde{p}(x) = c_0 + c_1 x \quad (\text{A.21})$$

From the boundary condition at $x = 0$,

$$c_0 = 0 \quad (\text{A.22})$$

and from the boundary condition at $x = L$,

$$c_1 = \frac{1}{L} \tilde{p}(L) \quad (\text{A.23})$$

$$\tilde{P}(x) = \tilde{p}(L) \frac{x}{L} \quad (\text{A.24})$$

$$\varepsilon_1 \delta_1 \frac{dL}{dt} = \frac{-k_1 \delta_1}{\mu} \frac{dP_1}{dx} I_{x=L} \quad (\text{A.25})$$

$$\varepsilon_2 \delta_2 \frac{dL}{dt} = \frac{-k_2 \delta_2}{\mu} \frac{dP_2}{dx} I_{x=L} \quad (\text{A.26})$$

Add together

$$(\varepsilon_1 \delta_1 + \varepsilon_2 \delta_2) \frac{dL}{dt} = \frac{-1}{\mu} \frac{d\tilde{P}}{dx} I_{x=L} \quad (\text{A.27})$$

$$(\varepsilon_1 \delta_1 + \varepsilon_2 \delta_2) \frac{dL}{dt} = \frac{-1}{\mu L} \tilde{P}(L) \quad (\text{A.28})$$

$$(\varepsilon_1 \delta_1 + \varepsilon_2 \delta_2) \frac{dL}{dt} = \frac{(\delta_1 k_1 P_{c1} + \delta_2 k_2 P_{c2})}{\mu L} \quad (\text{A.29})$$

Introduce another new variable

$$A = \frac{(\delta_1 k_1 P_{c1} + \delta_2 k_2 P_{c2})}{\mu(\varepsilon_1 \delta_1 + \varepsilon_2 \delta_2)} \quad (\text{A.30})$$

$$\frac{d\left(\frac{L^2}{2}\right)}{dt} = A \quad (\text{A.31})$$

$$L(t) = \sqrt{2At} \quad (\text{A.32})$$

$$L^2 = 2At \quad (\text{A.33})$$

If the two plies are the same,

$$A_0 = \frac{2\delta_1 k_1 p_{c1}}{\mu(2\varepsilon_1 \delta_1)} = \frac{k_1 p_{c1}}{\mu \varepsilon_1} \quad (\text{A.34})$$

So the equation reduces to Darcy's law.

$$p_2 = \frac{1}{\delta_2 k_2} \left[\frac{\tilde{p}(L)x}{L} - \delta_1 K_1 p_1 \right] \quad (\text{A.35})$$

$$p_1 - p_2 = p_1 \left(1 + \frac{\delta_1 K_1}{\delta_2 K_2} \right) - \frac{\tilde{p}(L)x}{\delta_2 k_2 L} \quad (\text{A.36})$$

So

$$\frac{d^2 p_1}{dx^2} = \frac{1}{\delta_1 K_1 R} \left[p_1 ()_1 - \frac{\tilde{p}(L)x}{\delta_2 K_2 L} \right] \quad (\text{A.37})$$

which is of the form

$$p_1'' - \alpha^2 p_1 = cx \quad (\text{A.38})$$

where

$$\alpha^2 = \frac{()_1}{\delta_1 K_1 R} = \frac{1}{R} \left(\frac{1}{\delta_1 K_1} + \frac{1}{\delta_2 k_2} \right) \quad (\text{A.39})$$

and

$$c = \frac{-\tilde{p}(L)}{\delta_1 K_1 R \delta_2 K_2 L} \quad (\text{A.40})$$

Solution is of the form

$$p_1 = a_1 \cosh \alpha x + b_1 \sinh \alpha x + Dx \quad (\text{A.41})$$

where

$$\begin{aligned} -\alpha^2 D &= C \\ D &= \frac{-c}{\alpha^2} \end{aligned} \quad (\text{A.42})$$

Applying the boundary conditions

$$p_1(L) = -P_{cl} = b_1 \sinh \alpha L - \frac{c}{\alpha^2} L \quad (\text{A.43})$$

$$b_1 = \frac{\frac{cL}{\alpha^2} - P_{cl}}{\sinh \alpha L} \quad (\text{A.44})$$

$$p_1 = \frac{-cx}{\alpha^2} + \frac{\frac{cL}{\alpha^2} - P_{cl}}{\sinh \alpha L} \sinh \alpha x \quad (\text{A.45})$$

$$p_2 = \frac{1}{\delta_2 K_2} \left[\frac{\tilde{p}(L)x}{L} - \delta_1 K_1 \left[\frac{-cx}{\alpha^2} + \frac{cL}{\alpha^2 - p_{c1}} \sinh \alpha x \right] \right] \quad (\text{A.46})$$

More generally,

$$p_1(x) = - \left(\frac{\delta_1 K_1 p_{c1} + \delta_2 k_2 p_{c2}}{\delta_1 k_1 + \delta_2 k_2} \right) \frac{x}{L} - \frac{\delta_2 K_2}{(\delta_1 K_1 + \delta_2 K_2)} (p_{c1} - p_{c2}) \frac{\sinh \alpha x}{\sinh \alpha L} \quad (\text{A.47})$$

$$p_2(x) = - \left(\frac{\delta_1 K_1 p_{c1} + \delta_2 k_2 p_{c2}}{\delta_1 k_1 + \delta_2 k_2} \right) \frac{x}{L} + \frac{\delta_2 K_2}{(\delta_1 K_1 + \delta_2 K_2)} (p_{c1} - p_{c2}) \frac{\sinh \alpha x}{\sinh \alpha L} \quad (\text{A.48})$$

So flow is always from in the direction from 2 to 1 (having previously assumed higher capillary pressure in 1). This is consistent with the dye experiment results. However, this model ends up predicting a weighted average behavior for the two-ply material, rather than the observed enhancement. An analytical pseudo 1-D model is insufficient to explain the behavior. A more rigorous 2-D model may be more successful.

Appendix B: MATLAB Code

Wickingtest.m was the code used to obtain a 3-D graph from an NMR data file.

It uses moviedata.m, which converts NMR data into a 2-D image, and rota.m, which rotates that image into the proper orientation.

wickingtest.m

```
function wickingtest(file,left,right,top,bottom,angle)
for n= 1:128
    image=moviedata(file,n);
    wangle=rota(image,angle);
    for j=1:(right-left)
        points(j,1:(bottom-top)+1)=wangle(top:bottom,left+j);
    end
    tempsum=sum(points);
    average(n,1:(bottom-top)+1)=tempsum/(right-left);

end
figure()
surf (average)
```

moviedata.m

```
function image= moviedata(infile,nselect)
%nselect=30
% load bruker 2d fid,
% calculate patterson function
% infile: filename of bruker fid file
% n2: size in x1
% n1: size in x2
%image: data output

% infile=input('enter filename of Bruker time data: ','s');

disp('# of complex data points in t2 [128]: ');
n2=128

disp('# of data points in t1 [128]: ');
n1=128
```

```

n2=2*n2; %double since one complex is stored as two reals

disp('# of movie frames [128]: ');
n3=128

%nselect=input('enter movie frame to be studied: ');

ntotal=n1*n2*n3;
infile
nselect
disp(' ')
disp('reading data')
fid=fopen(infile,'r','l'); %this may be changed depending on data transfer 'l' to 'b'
data_vekt=fread(fid,ntotal,'int32');
st=fclose(fid);

disp('starting loading into matrix at data point:')
icount=(nselect-1)*n1*n2 + 1

for ll=1:1:n1
    for kk=1:1:n2
        data_s(kk,ll)=data_vekt(icount);
        icount=icount+1;
    end
end

disp(' ')
disp('converting Bruker data into complex matrix')

time_data=data_s(1:2:n2-1,:)+ data_s(2:2:n2,:)*i;
n2=n2/2; % now n2 is describing complex dimension
clear data_s

disp(' ')
disp(' doing 2d-fft')

image=fft2(time_data,n2,n1); %one dimension real one is complex
%shifting data % FFT shift does not do the job, is there a better algorithm than the
% one used here?
disp('shifting result of 2d-fft')
image_a=image(1:(n2/2),1:(n1/2));
image_b=image(1:(n2/2),(n1/2+1):n1);
image_c=image((n2/2+1):n2,1:(n1/2));
image_d=image((n2/2+1):n2,(n1/2+1):n1);

image(1:(n2/2),1:(n1/2))=image_d;
image(1:(n2/2),(n1/2+1):n1)=image_c;
image((n2/2+1):n2,1:(n1/2))=image_b;
image((n2/2+1):n2,(n1/2+1):n1)=image_a;

%free memory

clear image_a

```

```

clear image_b
clear image_c
clear image_d

disp(' doing magnitude calculation')
image=abs(image);

disp(' ')
disp('plotting image function')

%figure;
%imagesc(image);
%colorbar;
%colormap(gray(64));
%title(infile);
%drawnow;

disp(' ')
disp('image function stored in workspace as "image"')
disp('image function dimensions stored in workspace as "n1","n2"')

disp('calculating phase suppressed time data')
%time_data=abs(time_data);
time_data=time_data.*time_data;

% the square must be referred to single Matrix -Element and not to entire Matrix
% cf. Proof of Wiener Khintchin Theorem in B. Traubs thesis:
% for the proof  $|F(s)|^2 = F(s) * F(s)$ 
% this holds only for  $F.*F$  and not for  $F*F$  !!!!!
% also: phase information is lost by squaring individual complex matrix entries and
% not the matrix.
disp(' ')
disp(' doing 2d-fft')

patterson=fft2(time_data,n2,n1); %one dimension real, one is complex
%shifting data % FFT shift does not do the job, is there a better algorithm than the
% one used here?
disp('shifting result of 2d-fft')
patterson_a=patterson(1:(n2/2),1:(n1/2));
patterson_b=patterson(1:(n2/2),(n1/2+1):n1);
patterson_c=patterson((n2/2+1):n2,1:(n1/2));
patterson_d=patterson((n2/2+1):n2,(n1/2+1):n1);
%patterson=0;
patterson(1:(n2/2),1:(n1/2))=patterson_d;
patterson(1:(n2/2),(n1/2+1):n1)=patterson_c;
patterson((n2/2+1):n2,1:(n1/2))=patterson_b;
patterson((n2/2+1):n2,(n1/2+1):n1)=patterson_a;

%free memory

clear patterson_a

```

```

clear patterson_b
clear patterson_c
clear patterson_d

disp('infile ')
disp(' doing magnitude calculation')
patterson=abs(patterson);

disp(' ')
disp('plotting patterson function')

%figure;
%imagesc(patterson);
%colorbar;
%colormap(gray(64));
%title(infile);
%drawnow;

disp(' ')
disp('patterson function stored in workspace as "patterson"')
disp('patterson function dimensions stored in workspace as "n1","n2"')

clear st %clear unwanted variables
clear fid
clear infile

end

```

rota.m

```

% rotmat.m
% by Hakon Gudbjartsson, 03/25/95
% Purpose: rotate a matrix
% Usage: rotated_matrix=rotate(matrix,angle);
% Note : clockwise is the positive sense of alpha

function z=rotat(a,alpha)
z=a;
if alpha~=0
    Nx=length(a(1,:));
    Ny=length(a(:,1));
    Cx=Nx/2+0.5;
    Cy=Ny/2+0.5;

```

```

[x y]=meshgrid(1:Nx,1:Ny);
y=x';

nx=(x-Cx)*cos(alpha*pi/180)+(y-Cy)*sin(alpha*pi/180)+Cx;
ny=-(x-Cx)*sin(alpha*pi/180)+(y-Cy)*cos(alpha*pi/180)+Cy;

nx=nx-(nx-1).*(nx<1);
ny=ny-(ny-1).*(ny<1);
nx=nx-(nx-Nx+1).*(nx>Nx-1);
ny=ny-(ny-Ny+1).*(ny>Ny-1);
x=floor(nx);
y=floor(ny);
dx=nx-x;
dy=ny-y;

a=reshape(a.',1,Nx*Ny);

for ii=1:Nx
    aa=a(Nx*(y(ii,:)-1)+x(ii,:));
    bb=a(Nx*y(ii,:)+x(ii,:));
    cc=a(Nx*(y(ii,:)-1)+x(ii,:)+1);
    dd=a(Nx*y(ii,:)+x(ii,:)+1);
    z(ii,1:Nx)=(aa.*(1-dy(ii,:))+dy(ii,:).*bb).*(1-dx(ii,:)) + ...
        (cc.*(1-dy(ii,:))+dy(ii,:).*dd).*dx(ii,:);
end

z=reshape(z,Ny,Nx);
end

```

REFERENCES

- (1) Alava M, Dube, M and Rost, M., "Imbibition in Disordered Media" *Advances in Physics*. **2004**, 53, 2, 83–175
- (2) Hamroui, A., and Nylander, T., "Analytical Approach for the Lucas–Washburn Equation" *J. Colloid. Interface Sci.*, **2002**, 250, 415.
- (3) Bear, J. ,*Dynamics of Fluids in Porous Media*, American Elsevier, **1972**
- (4) Miller, B., "Critical Evaluation of Upward Wicking Tests", *International Nonwovens Journal*. **2000**, 9, 35-40.
- (5) Smook, G., *Handbook for Pulp and Paper Technologists*, 2nd ed. Angus Wilde Publications, Vancouver, B.C., **1992**
- (6) Nanko, H and Wu J., "Mechanisms of Paper Shrinkage During Drying" *International paper physics conference*. **1995** 103-113
- (7) Lyne, M. "Wetting and the Penetration of Liquids into Paper", **2002**, *Handbook of Physical Testing of Paper* (2nd ed, pp 303-332)
- (8) Alava, M., Dube, M. Chabot, B. and Daneault, C., "Fundamentals of Fluid Front Roughening in Imbibition" *Pulp and Paper Canada*, **2005**, 106, 9, 25-28
- (9) Topgaard, D. and Söderman, O., "Diffusion of Water Absorbed in Cellulose Fibers Studied with 1H NMR" *Langmuir* **2001**, 17, 2694-2702.
- (10) Pan, N. and Zhong, W., "Fluid Transport Phenomena in Fibrous Materials" *Textile Progress*, **2006** 38, 2, p 1-93
- (11) Marchal, J., "Modeling Capillary Flow in Complex Geometries", *Textile Research Journal*. **2001**, 71, 813-821.
- (12) Simile, C., "Critical Evaluation of Wicking in Performance Fabrics" **2004** Georgia Tech
- (13) Staples T. and Shaffer D., "Wicking Flow in Irregular Capillaries" *Colloids and Surfaces A* **2002** 239-250
- (14) Leisen J., Hojjatie, B., Coffin, D., Lavrykov, S., Ramarao, B., and Beckham, H., "Through-Plane Diffusion of Moisture in Paper Detected by Magnetic Resonance Imaging", *Industrial and Engineering Chem. Res.* **2002**, 41(25), 6555-6565
- (15) www.cis.rit.edu/htbooks/mri/
- (16) Harding, S. G., D. Wessman, S. Stenström, and L. Kenne. , "Water Transport During the Drying of Cardboard Studied by NMR Imaging and Diffusion Techniques". *Chem. Eng. Sci.* **2001** 56 5269-5281.

- (17) Akshaya J. and Krishna G., "Flow Porometry: What Can Flow Porometry Do For Us?"
2002 Porous Materials, Inc.